

NAVAL POSTGRADUATE SCHOOL

Monterey, California



THESIS

DEVELOPMENT, CORRELATION AND UPDATING OF A FINITE ELEMENT MODEL OF THE OH-6A HELICOPTER

by

Michael R. Pampalone

December 1996

Thesis Advisor:
Second Reader:

Joshua H. Gordis
E. Roberts Wood

Approved for public release; distribution is unlimited.

19980102 037

DTIC QUALITY INSPECTED 4

REPORT DOCUMENTATION PAGE

Form Approved OMB No. 0704-0188

Public reporting burden for this collection of information is estimated to average 1 hour per response, including the time for reviewing instruction, searching existing data sources, gathering and maintaining the data needed, and completing and reviewing the collection of information. Send comments regarding this burden estimate or any other aspect of this collection of information, including suggestions for reducing this burden, to Washington Headquarters Services, Directorate for Information Operations and Reports, 1215 Jefferson Davis Highway, Suite 1204, Arlington, VA 22202-4302, and to the Office of Management and Budget, Paperwork Reduction Project (0704-0188) Washington DC 20503.

1. AGENCY USE ONLY (Leave blank)		2. REPORT DATE December 1996	3. REPORT TYPE AND DATES COVERED Master's Thesis
4. TITLE AND SUBTITLE Development, Correlation and Updating of a Finite Element Model of The OH-6A Helicopter			5. FUNDING NUMBERS
6. AUTHOR(S) Pampalone, Michael R.			
7. PERFORMING ORGANIZATION NAME(S) AND ADDRESS(ES) Naval Postgraduate School Monterey CA 93943-5000			8. PERFORMING ORGANIZATION REPORT NUMBER
9. SPONSORING/MONITORING AGENCY NAME(S) AND ADDRESS(ES)			10. SPONSORING/MONITORING AGENCY REPORT NUMBER
11. SUPPLEMENTARY NOTES The views expressed in this thesis are those of the author and do not reflect the official policy or position of the Department of Defense or the U.S. Government.			
12a. DISTRIBUTION/AVAILABILITY STATEMENT Approved for public release; distribution is unlimited.			12b. DISTRIBUTION CODE
13. ABSTRACT (maximum 200 words) This thesis is part of the helicopter research program established at The Naval Postgraduate School (NPS). NPS currently has two OH-6A light observation helicopters which were obtained from the U. S. Army. One of these is dedicated to ground vibration testing and dynamics research. Previous research on the OH-6A at NPS established baseline vibration test data. The data includes natural frequencies, principal mode shapes and damping characteristics. This thesis continues previous research of the OH-6A and develops a detailed finite element model to be used in future helicopter dynamics research at NPS. The model is based on an MSC/NASTRAN finite element model of a similar aircraft obtained from the McDonnell Douglas Helicopter Company. Both the nose and empennage were modified to represent the structural characteristics of the test article. Due to lack of structural design data, model mass updating was performed using previously obtained test data and a design sensitivity approach. The updated model natural frequencies agree well with the test data.			
14. SUBJECT TERMS Helicopter, OH-6A, Vibration Analysis, Finite Element Modeling, Modal Analysis, Natural Frequencies, Mode Shapes, NASTRAN, Sensitivity Analysis, Modal Assurance Criterion, MAC			15. NUMBER OF PAGES 111
			16. PRICE CODE
17. SECURITY CLASSIFICATION OF REPORT Unclassified	18. SECURITY CLASSIFICATION OF THIS PAGE Unclassified	19. SECURITY CLASSIFICATION OF ABSTRACT Unclassified	20. LIMITATION OF ABSTRACT UL

NSN 7540-01-280-5500

Standard Form 298 (Rev. 2-89)
Prescribed by ANSI Std. Z39-18 298-102

Approved for public release; distribution is unlimited.

**DEVELOPMENT, CORRELATION AND UPDATING OF A FINITE
ELEMENT MODEL OF THE OH-6A HELICOPTER**

Michael R. Pampalone
Lieutenant, United States Navy
B.S., The Citadel, 1988

Submitted in partial fulfillment
of the requirements for the degree of

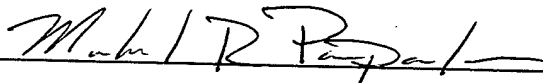
MASTER OF SCIENCE IN MECHANICAL ENGINEERING

from the

NAVAL POSTGRADUATE SCHOOL

December 1996

Author:

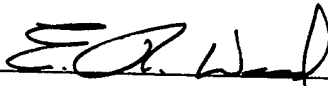


Michael R. Pampalone

Approved by:



Joshua H. Gordis, Thesis Advisor



E. Roberts Wood, Second Reader



Terry R. McNelley, Chairman
Department of Mechanical Engineering

ABSTRACT

This thesis is part of the helicopter research program established at The Naval Postgraduate School (NPS). NPS currently has two OH-6A light observation helicopters which were obtained from the U. S. Army. One of these is dedicated to ground vibration testing and dynamics research.

Previous research on the OH-6A at NPS established baseline vibration test data. The data includes natural frequencies, principal mode shapes and damping characteristics. This thesis continues previous research of the OH-6A and develops a detailed finite element model to be used in future helicopter dynamics research at NPS.

The model is based on an MSC/NASTRAN finite element model of a similar aircraft obtained from the McDonnell Douglas Helicopter Company. Both the nose and empennage were modified to represent the structural characteristics of the test article. Due to lack of structural design data, model mass updating was performed using previously obtained test data and a design sensitivity approach. The updated model natural frequencies agree well with the test data.

TABLE OF CONTENTS

I. INTRODUCTION	1
II. THE MCDONNELL DOUGLAS OH-6A	5
A. CHARACTERISTICS OF THE OH-6A	5
B. THE OH-6A AT NPS	6
1. Acquisition	6
2. Overview of Previous Testing	6
C. MOTIVATION FOR MODELING THE OH-6A	7
III. VIBRATION THEORY	9
A. HELICOPTER VIBRATIONS	9
1. Main Rotor Vibrations	10
2. Random Aerodynamic Excitations	12
3. Self-Excited Vibrations	12
B. SINGLE DEGREE OF FREEDOM (SDOF) SYSTEMS	13
1. Free Response	13
2. Forced Response	14
C. MODAL ANALYSIS	17
D. RIGID BODY MODES	20
IV. FINITE ELEMENT MODELING	23
A. THE SIMPLE ROD ELEMENT	23
1. Discretization	23
2. Determine Mass and Stiffness Matrices	26
3. Modeling Multi-Element Structures	29
B. ASSOCIATED ERRORS	31
V. THE OH-6A FINITE ELEMENT MODEL	37
A. STRUCTURAL MODEL	37
1. Nose Section	39

2.	Empennage Section	40
3.	Structural Elements	44
a.	Rod Element	45
b.	Bar Element	46
c.	Shear Panel Element	48
d.	Rigid Elements	49
B.	MASS MODEL	50
VI.	COMPARISON OF RESULTS	57
A.	MODAL ASSURANCE CRITERION	57
B.	MATRIX REDUCTION	60
C.	COMPARISON PROCEDURES	63
D.	MODE SHAPES	65
1.	Lateral Modes	65
2.	Vertical Modes	68
3.	Torsional Mode	72
VII.	CONCLUSIONS AND RECOMMENDATIONS	75
A.	CONCLUDING REMARKS	75
B.	RECOMMENDATIONS FOR FURTHER STUDY	77
1.	Improvements in the Experimental Data	77
2.	Improvements in the FEM	78
APPENDIX A.	EXPERIMENTAL MODE SHAPE PLOTS	79
APPENDIX B.	MODE SHAPE EXTRACTION PROGRAM	81
APPENDIX C.	REDUCED MODE SHAPE DATA	83
APPENDIX D.	MAC CALCULATION PROGRAM	85
APPENDIX E.	NASTRAN FORMATTED EMPENNAGE DATA	87
LIST OF REFERENCES	97
INITIAL DISTRIBUTION LIST	99

ACKNOWLEDGMENTS

This thesis could not have been completed without the help of several individuals. First, I would like to thank Dr. Moe Toossi at McDonnell Douglas Helicopters who provided the original finite element model on which this FEM is based. The time I spent at the Mesa, Arizona facility proved to be an invaluable experience.

I would also like to thank my thesis advisor, Professor Gordis, who provided a tremendous amount knowledge in the area of vibrations and invaluable insight into the inner workings of NASTRAN. Thanks also go to Professor Wood who provided me with a working knowledge of helicopter dynamics and of the OH-6A airframe.

Finally, I'd like to thank my wife Elizabeth and sons Justin and Collin who put up with many late nights and 'working weekends.' I could not have accomplished any of this without their love and support.

I. INTRODUCTION

Vibration reduction has long been a primary concern of helicopter design engineers. The inherently vibratory nature of the complex rotating machinery associated with helicopters has made this task particularly difficult. Additionally, ever increasing cost and lower vibration tolerance of complex helicopter avionics systems puts even greater emphasis on vibration level reduction. An accurate finite element model (FEM) is invaluable in developing modern aircraft which minimize vibrations while achieving higher performance.

With the revolution in computing capability over the last several years, the FEM has become an integral part of structural dynamics research. This is especially true in the study of helicopter vibrations. Prior to the development of robust finite element computer models, dynamics analysis was completed using iterative tests on full scale models. The costs associated with developing a full scale model of a modern helicopter make this approach impractical. The FEM provides a means to conduct preliminary dynamic analysis relatively inexpensively prior to conducting a full scale test. This approach greatly reduces development costs. The FEM is also used to test and develop new aircraft components and airframe modifications and to investigate vibration problems which are discovered after production. This not only reduces the cost of development but also the time associated with analyzing dynamic response.

The purpose of this thesis was to develop a finite element model of the OH-6A helicopter. The Naval Postgraduate School (NPS) recently acquired two of the McDonnell Douglas aircraft. One aircraft is dedicated to helicopter dynamics research. A

full scale vibration test of this helicopter established the primary natural frequencies and mode shapes between zero and 45 Hz. and compared them to data provided by McDonnell Douglas Helicopter Company (MDHC). The FEM developed in this thesis was created to closely match the results of this test in order to allow further research on a validated model.

Prior to the development of a finite element model, the nature of the vibratory forces acting on the structure must be understood. Chapter III of this thesis discusses harmonically forced vibrations in general and the unique characteristics of helicopter vibrations specifically. There is also a discussion of the mathematical techniques used to solve the vibration problem in multi-DOF systems.

In Chapter IV, the method of finite element modeling is discussed. The development of the simplest of the finite elements, the rod, is used to introduce the concept of discretization and interpolation. The errors associated with the use of finite elements are also discussed.

The remainder of the thesis discusses the OH-6A FEM. MDHC was able to provide a model which they had developed for a similar aircraft. This model was then modified to match the test platform at NPS. The result is a 1774 element finite element model. It is written using the NASTRAN finite element code which is developed and supported by the MacNeal-Schwendler Corporation.

The FEM was modified in three separate steps. First, the structural model was created. The modifications were complicated by the absence of accurate structural design data for the test platform. The FEM was completed using physical measurements of the

helicopter at NPS. In addition, the physical properties of the internal structural components were assumed based on the model provided by MDHC.

Once the structural model was completed, the mass model was then developed. As with the structural model, the creation of the mass model was complicated by the absence of mass data for the newly created empennage structure. For this reason, the mass distribution on the tail was determined using a sensitivity analysis approach in conjunction with measured frequencies. This was simplified by using a single point mass with rotational components. It was strategically placed near the C.G. of the empennage section which was determined by visual inspection. The result was a set of frequencies which closely match test data. Chapter V outlines the procedures taken in the development of both the structural and mass components of the FEM. It also includes a discussion of the design sensitivity approach.

The final step in the development of an accurate model is mode shape correlation. The analytical mode shapes were compared to the test data using the Modal Assurance Criterion (MAC). Prior to comparing the mode shapes, however, the analytical model was reduced to the same size as the test model. This was accomplished using NASTRAN and the built-in static reduction method. The results of the correlation are given in Chapter VI. This is preceded by a discussion of the MAC and the theory of static matrix reduction.

The FEM developed matched the test frequencies quite well. There were some discrepancies in the mode shapes. This can be attributed to the small number of data points taken on the test platform and the large static reduction required in the analytical

model to match it. There was also a noticeable coupling of the landing skids in several modes of the analytical model. This was not noted in a previous test conducted by MDHC [Ref. 2] or the test at NPS. It also could have had an effect on the calculated frequencies. Overall, the updated model provides an accurate tool for calculating dynamic response for the OH-6A helicopter.

II. THE MCDONNELL DOUGLAS OH-6A

A. CHARACTERISTICS OF THE OH-6A

The OH-6A is a single engine, four bladed dual piloted helicopter. The aircraft is manufactured by McDonnell Douglas Helicopter Company for the U. S. Army. Its primary function is as an observation platform. It is equipped with a two bladed tail rotor and oleo-damped skid-type landing gear. The empennage is an asymmetrical V-tail [Ref. 1].

The main rotor rotates at 483 RPM. The tail rotor RPM is 3029. The 1/rev (1P) frequency is, therefore, approximately 8 Hz. with the 4P frequency at close to 32 Hz. High frequency excitation from the tail rotor occurs at approximately 50 Hz.

The airframe is of semi-monocoque construction consisting of frames, bulkheads and stringers covered with stressed skin [Ref. 2:p. 10]. The primary structural components are the fuselage, tailboom and empennage which include a primary and secondary structure consisting of all metal, metal and fiberglass, and transparent plastic components [Ref. 3:p. 17]. The principal structural component of the fuselage is the reinforced floor center section. Both the fuselage and tailboom are metal, riveted structures incorporating aluminum alloy frames, stainless steel and titanium bulkheads, canted frames, channel members, beams, structure rings, ribs, stiffeners, doublers, longerons and stringers [Ref. 1].

B. THE OH-6A AT NPS

1. Acquisition

In October, 1995 The Naval Postgraduate School obtained two OH-6A helicopters from the U. S. Army. The acquisition of the helicopters was a first step in launching a rotor craft dynamics program at the school. One of the helicopters is designated as a dynamics laboratory test platform. The other is designated to remain operational. It is part of a proposed flight test center being organized by CAPT Tom Hoivik, USN (Ret.) of the Operations Research department at NPS [Ref. 3:p. 17].

2. Overview of Previous Testing

Initial research on the OH-6A involved performing a full-scale vibration test of the laboratory test platform. This test was performed by LT John Harris at NPS in the spring of 1996 [Ref. 3]. His research involved determining the natural frequencies, mode shapes and damping characteristics of the helicopter at frequencies between zero and 45 Hz. Once principal modes were identified, they were then compared to data obtained from MDHC.

The six natural frequencies which were detected in the designated frequency range are shown in Table 2.1. These correlated well with the data obtained from McDonnell Douglas. Mode shapes were developed for four of these frequencies. They are reproduced in Appendix A of this thesis.

Table 2.1. Experimental Natural Frequencies. After Ref. [3].

Mode	Frequency (Hz.)
1 st Lateral	9.32
1 st Vertical	9.97
1 st Torsional	15.01
Aft Vertical	15.61
2 nd Vertical	21.83
2 nd Lateral	27.48
Unnamed	44.84

C. MOTIVATION FOR MODELING THE OH-6A

The OH-6A is a relatively simple aircraft in comparison with modern military helicopters. It has been operational for 30+ years and there is significant data available concerning its dynamic response. This makes it an ideal aircraft to study. The completion of the full-scale vibration test was a first step in understanding the vibratory response of the helicopter. Development of the FEM further enhances corporate knowledge of the response of the OH-6A and of helicopter dynamics in general.

The completed finite element model is an excellent teaching tool. Once the process required to build a simple FEM is understood, complex FEM can then be developed. Students conducting research into more complex aircraft structures can use this model as an introduction into helicopter dynamics. A thorough understanding of this

validated model will provide the basic knowledge required to develop a FEM of a prototype or concept aircraft.

The acquisition of a helicopter dedicated to vibrational testing coupled with a validated in-house FEM of that helicopter greatly enhances the prestige of the school as a helicopter dynamics research facility. Completion of the full-scale vibration test of the OH-6A was a first step toward establishing a helicopter dynamics program at NPS. Developing a FEM for the helicopter increases the viability of the program.

III. VIBRATION THEORY

A. HELICOPTER VIBRATIONS

Vibration reduction in helicopters is necessary in order to both reduce fatigue on sensitive avionics and airframe components and to enhance crew and passenger comfort. In order to achieve a reduction in vibration levels, the source of vibrations must be known. With this information, the aircraft is then designed with the principal structural frequencies offset from the driving frequencies. Additionally, damping techniques can be implemented to reduce the amplitude of the airframe response. These can be either traditional passive techniques, using isolation mounts and vibration absorbers, or more advanced active damping techniques, using inputs to the main rotor blades.

Helicopters experience vibrations from a few primary sources. Most vibrations transmitted to the airframe are associated with the main and tail rotors [Ref. 3:p. 10]. These frequencies are normally multiples of the rotor speed. Other sources of vibration are associated with internal machinery such as engines and transmission components. These are normally higher frequency. There are also vibrations associated with random aerodynamic excitations due to wind gusts and changes in flight profile as well as self-induced vibrations.

1. Main Rotor Vibrations

Blade forces and moments are transmitted to the airframe at the rotor hub.

Typically, the hub is designed so that lead-lag and flapping bending moments at the blade root are negligible. The result of this is that only the $N \times \text{rpm}$, or NP, (N = number of blades) harmonics are transmitted to the airframe from the rotor [Ref. 4:p. 2]. Studies have shown that the NP and 1P frequencies dominate the excitation. All of the other frequencies are filtered out by the rotor system. This assumes that all of the blades are balanced, the helicopter is in steady state flight, and each blade has the same time history as its neighboring blades.

The frequency of greatest concern transmitted from the rotor hub is typically the NP frequency. This is called the blade passage frequency [Ref. 4:p. 19]. The dependence of cockpit vibration levels on airspeed is shown in Figure 3.1. The NP vibrations are a major source of these levels. They are the result of higher harmonic loading on the blades [Ref. 4:p. 2]. These loads are induced by a variety of conditions including: impingement from the rotor wake, blade vortex intrusion, and retreating blade stall and advancing blade compressibility phenomena.

Rotor wake impingement on the blade disk is observed at low airspeeds. At low speeds, the rotor wake remains close to the helicopter. The resulting interference on the rotor causes the higher harmonic loads. The loads fall off as the helicopter increases airspeed and the rotor wash is swept behind the aircraft. This is observed in the 70 - 90 knot region in Figure 3.1.

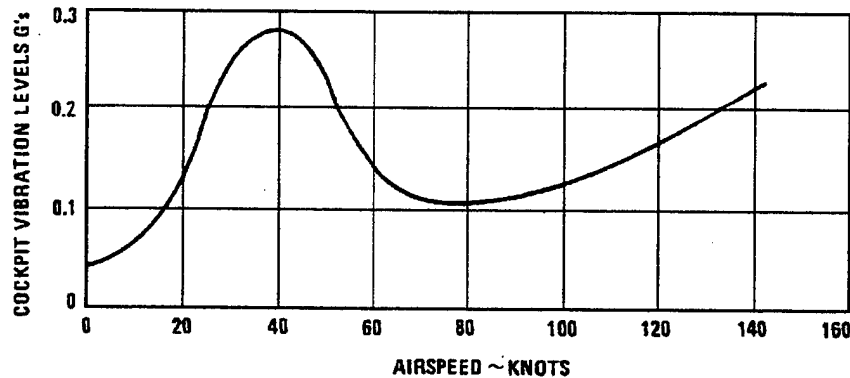


Figure 3.1. Helicopter Vibration vs. Airspeed. From Ref.[4].

Blade vortex interaction refers to the interference caused by the blades passing through the vortices induced by the preceding blade. These effects are normally felt during deceleration and descent maneuvers. The loads created by this effect also manifest themselves as 4P vibrations on the airframe.

The other major cause of 4P vibration occurs at higher airspeeds. As the aircraft increases airspeed above about 80 knots, retreating blade stall and advancing blade compressibility effects begin to appear. The higher harmonic loads induced result in increased 4P vibrations with increase in forward airspeed.

Some blade loading conditions will excite the airframe at a frequency other than 4P. For instance, a 1P vibration indicates a blade track and balance problem. It is normally corrected by adjusting the blade track using either weights on the rotor hub, changes to the pitch control rod length or a combination of both. Also, a 2P vibration is possible. This is felt as a lateral excitation of the airframe and is associated with a blade damper malfunction. The 1P and 2P frequencies can be corrected by maintenance, so they are not design critical as is the 4P vibration.

2. Random Aerodynamic Excitations

Random aerodynamic excitation is the result of the airflow across the airframe.

Airflow induced by the main rotor is broadband in nature. It can excite a any given number of natural frequencies of the airframe at certain airspeeds. In order to avoid this possibility, the airflow can be redirected using fairings. [Ref. 4:p. 3]. Wind gusts and airflow conditions induced during abrupt aircraft maneuvers can also cause excitation of the airframe. These conditions are transient in nature and are, therefore, not as critical as the rotor wash condition.

3. Self-Excited Vibrations

Self-excited vibrations result from aerodynamic or mechanical instability. In this situation, the vibratory motion grows exponentially without bound over time. The damping force in this case is negative. Consider the following example [Ref. 5:p. 52]. The equation of motion of a system is modeled as:

$$m\ddot{x} + c\dot{x} + kx = \gamma\dot{x}. \quad (3.1)$$

In this case, the driving force is a function of velocity. The equation can now be rewritten as:

$$m\ddot{x} + (c - \gamma)\dot{x} + kx = 0. \quad (3.2)$$

The system is stable if the damping term ($c - \gamma$) is positive. If that term becomes negative then $\zeta = \frac{c - \gamma}{2m\omega} < 0$ and the solution is of the form:

$$x_{(t)} = Ae^{-\zeta\omega t} \sin(\omega_d t + \phi). \quad (3.3)$$

The exponential term grows over time, and the displacement is unbounded. The best known occurrence of this situation in helicopters is the ground resonance condition, a mechanical instability.

B. SINGLE DEGREE OF FREEDOM (SDOF) SYSTEMS

Most structures must be modeled using many - sometimes thousands of - degrees of freedom (DOF). In order to understand how these multiple DOF systems are excited, the SDOF model must first be studied. The solutions obtained from the simple model are then applied to larger models using a systematic modal analysis approach.

1. Free Response

The response of a structure to an initial disturbance without any external forcing function is the free response. As discussed in the previous section, the helicopter is subject to various harmonic loads. Understanding the free response of the structure however, is critical to the understanding of the response when a forcing function is applied (forced response). As will be seen, the solution to the forced response problem is a linear combination of the free response and a particular solution determined by the fractional form of the forcing function.

Consider the undamped SDOF system with mass (m) and spring constant (k). The equation of motion of the system is:

$$m\ddot{x} + kx = 0. \quad (3.4)$$

If the response of the system is considered to be harmonic, the solution is well documented and is given as [Ref. 5:p. 11]:

$$x = ae^{\pm\omega_j t}. \quad (3.5)$$

The amplitude of the response (a) is determined by the initial conditions imposed on the system. Assuming that $x_{(0)} = x_o$, $\dot{x}_{(0)} = \dot{x}_o$ and introducing the Euler's trigonometric identities [Ref. 6:p. 57], the solution becomes:

$$x = x_o \cos(\omega t) + \frac{\dot{x}_o}{\omega} \sin(\omega t). \quad (3.6)$$

2. Forced Response

The response of a structure subject to an external excitation is the forced response. The external driving forces of particular interest in the study of helicopter vibrations are harmonic and have the form:

$$F(t) = F_o \cos(\Omega t), \quad (3.7)$$

where Ω is the driving frequency. The equation of motion for the forced system is then written:

$$m\ddot{x} + kx = F(t). \quad (3.8)$$

The solution to Equation 3.8 is a linear combination of both the homogeneous (free response) solution (Equation 3.6) and the particular solution. The particular solution is found by assuming a form which is identical to the forcing function:

$$x_p = A_o \cos(\Omega t). \quad (3.9)$$

The response is then found by taking derivatives of Equation 3.9 and substituting into Equation 3.8. This equation can be solved for A_o . Combining the particular and homogeneous solution gives the total response of the harmonically forced structure:

$$A_1 \cos(\omega t) + A_2 \sin(\omega t) + \frac{F_o}{m(\omega^2 - \Omega^2)} \cos(\Omega t). \quad (3.10)$$

The solution is normally written in terms of the frequency ratio $r = \frac{\Omega}{\omega}$ and a normalized amplitude $U_o = \frac{F_o}{k}$. Equation 3.10 then becomes:

$$x = A_1 \cos(\omega t) + A_2 \sin(\omega t) + \frac{U_o}{1 - r^2} \cos(\Omega t). \quad (3.11)$$

As the driving frequency approaches the natural frequency of the system, the frequency ratio approaches unity. The assumed particular solution in this case is no longer valid. A different solution of the form $x_p = A_o t \sin(\Omega t)$ is assumed. This leads to the new solution:

$$x = \frac{1}{2} U_o \omega t \sin(\Omega t) + x_o \cos(\omega t) + \frac{\dot{x}_o}{\omega} \sin(\omega t). \quad (3.12)$$

As in the free response case, $x_{(0)} = x_o$, $\dot{x}_{(0)} = \dot{x}_o$.

This solution is plotted in Figure 3.2. The amplitude of the response in this case continues to increase over time. This is the resonant condition. It exists when the driving frequency is equal to the natural frequency of the structure. It is the goal in vibration

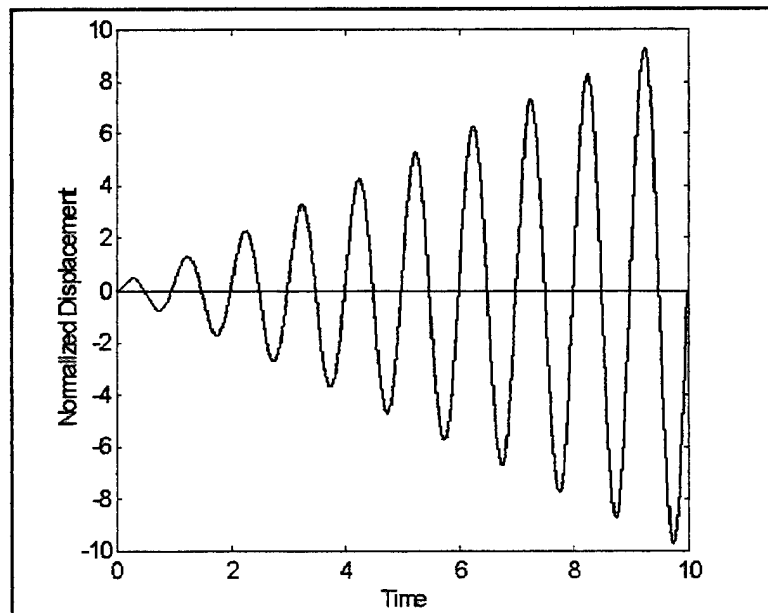


Figure 3.2. Forced Response of SDOF Undamped System

design to avoid resonance during steady state operation. From Equation 3.11, it is seen that when $r \neq 1$, the response amplitude is bounded. Therefore, if the structure is designed with natural frequencies which are offset from the driving frequency, the amplitude of the response will be finite. By understanding the possible forcing frequencies, it then becomes a matter of designing a structure with the normal modes offset.

It is important to note that this discussion does not include any mention of damping force. It is common in vibrational studies to ignore the damping force inherent in the structure. This is a conservative approach. For the case of the under damped structure, the damping force will act to reduce the amplitude of the response during resonant conditions. The damped structure will experience a transient excitation which decays exponentially followed by a steady state response frequency equal to the forcing frequency. A complete discussion on damped response can be found in most engineering vibration texts (e.g., Ref. [5], Chapter One).

C. MODAL ANALYSIS

Basic principles are easily demonstrated using the SDOF system previously discussed. Complex structures, however, are modeled with many - sometimes thousands of - DOF. In order to solve the associated equations, they must first be decoupled in a systematic fashion, then recombined to produce the response.

The modal analysis procedure is used to solve multiple DOF (MDOF) systems.

Consider a MDOF system which can be modeled using an NxN matrix equation:

$$[M]\{\ddot{x}\} + [K]\{x\} = \{F(t)\}. \quad (3.13)$$

The solution to this equation is found by first solving the homogeneous eigenvalue problem. The response is assumed to be of the form $\{x\} = \{\phi\}Ce^{j\omega t}$. This is substituted into Equation 3.13, which is rearranged to give:

$$[[M]^{-1}[K] - \omega^2[I]]\{\phi\} = \{0\}. \quad (3.14)$$

This is the eigenvalue problem. Observe that if the inverse of matrix $[[M]^{-1}[K] - \omega^2[I]]$ existed, Equation 3.14 could be pre-multiplied by that inverse matrix. This would give a trivial solution for $\{\phi\}$. Therefore, the inverse of the matrix must not exist if $\{\phi\}$ is non-zero. For this to be true, the determinant must be equal to zero. Solving for this condition gives a polynomial in ω^2 of order N. These are the natural frequencies of the system.

The mode shapes, $\{\phi\}$, are found by substituting the natural frequencies back into Equation 3.14. Each value of ω will give a unique Nx1 mode shape vector. The mode shapes are then combined to give:

$$[\Phi] = [\{\phi^1\}\{\phi^2\}...\{\phi^N\}]. \quad (3.15)$$

This is the modal matrix. It can be shown that the modal matrix is orthogonal to both the mass and stiffness matrix such that [Ref. 7]:

$$[\Phi]^T[M][\Phi] = [\tilde{M}]; \quad [\Phi]^T[K][\Phi] = [\tilde{K}], \quad (3.16)$$

where $[\tilde{M}]$ and $[\tilde{K}]$ are both diagonal matrices.

The original matrix equation can be transformed into a decoupled matrix equation. This is accomplished by assuming a new variable $\{x\} = [\Phi]\{q\}$ and pre-multiplying by $[\Phi]^T$ to give :

$$[\tilde{M}]\{\ddot{q}\} + [\tilde{K}]\{q\} = \{\tilde{F}\}. \quad (3.17)$$

In this new equation, the force vector $\{\tilde{F}\} = [\Phi]^T\{F\}$. The matrices $[\tilde{M}]$ and $[\tilde{K}]$ are now uncoupled (diagonal). The differential equation can therefore be written for each mode:

$$M_{ii}\ddot{q}_i + K_{ii}q_i = 0. \quad (3.18)$$

The solution to the modal equation is then easily solved using the techniques applied to SDOF systems. The solution for each of the uncoupled equations is:

$$q_i = A_i \cos(\omega_i t) + B_i \sin(\omega_i t) + q_{ip}(t). \quad (3.19)$$

In this case, $q_{ip}(t)$ is the particular equation. It depends on the form of the forcing function. For a harmonically excited system such as a helicopter subject to NP loading, q_{ip} is of the form given in Equation 3.9.

Once the modal equations are solved, the physical response is easily obtained. It is given above by $\{x\} = [\Phi]\{q\}$. It should be noted that in order to solve for the amplitude of the response, initial conditions must be applied. For systems which operate under a variety of conditions, this is not always a desirable approach. For such systems it is common to normalize the amplitudes in some deliberate manner in order to compare the response under various loading parameters.

D. RIGID BODY MODES

Unconstrained systems can have up to six modes in which none of the elastic elements deform. These are called rigid body modes. The rigid body modes occur when a structure is displaced without any deformation of its structural elements. An aircraft in flight is the commonly used example of such a structure.

In MDOF systems the stiffness matrix is related to the strain energy of each of the elements using Lagrange's equations. This is demonstrated in Chapter IV of this thesis. In most cases the strain energy is positive definite. This means that for any arbitrary displacement from the undisturbed condition a positive strain energy will result. If a system has one or more rigid body modes, no strain energy is produced with those

particular modes. In this case, the matrix $[K]$ becomes semi-positive definite and its determinate is zero [Ref. 6:p. 246].

From the eigenvalue problem in Equation 3.14 it is seen that if the determinant of $[K]$ is zero, there must be at least one solution where the natural frequency (ω) is zero as well. The mode shapes for the rigid body modes are found in the usual way of substituting the frequency back into the equation. When this is done, it is found that $\{\Phi^{RBM}\} \approx \{1\}$.

The number of rigid body modes will be equal to the degeneracies of $[K]$. For example, if there are six unrestrained DOF, then there will be six modes for which no strain energy will be generated when the structure is deflected. This leads to six rigid body modes.

IV. FINITE ELEMENT MODELING

A. THE SIMPLE ROD ELEMENT

The finite element method is used to model complicated structures. The structure is divided up into many small discrete elements. The response of the structure is then approximated by the motion of the element boundary points (nodes). Due to the systematic nature of the resulting mathematical equations, they are easily implemented on a modern microprocessor.

1. Discretization

In order to illustrate how a finite element model is constructed, consider a simple one dimensional (axial displacement only) rod element shown in Figure 4.1. The rod is length (l) with nodes (1,2) located at either

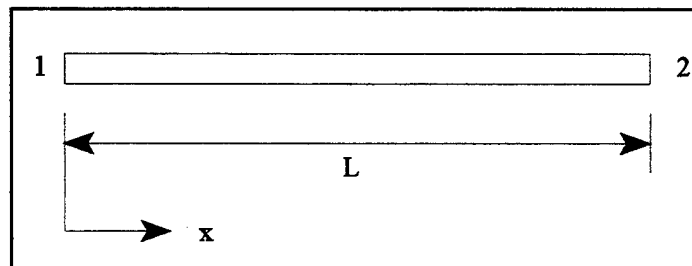


Figure 4.1. The Simple Rod Element

end. The local coordinate system on the rod is chosen with $x=0$ at node 1 and $x=L$ at node 2.

In order to determine the equations of motion for the rod, the time-independent (static) solution must first be obtained. Consider a small differential element shown in Figure 4.2. The force on the rod is given by $F = \sigma A$, where the unit stress (σ) is given by $\sigma = E\epsilon$. The unit strain (ϵ) is given by:

$$\epsilon = \frac{du_{(x)}}{dx}, \quad (4.1)$$

where $u_{(x)}$ is the time-independent displacement of the bar. Substitution then gives:

$$F = EA \frac{du_{(x)}}{dx}. \quad (4.2)$$

The time-independent displacement must satisfy this condition.

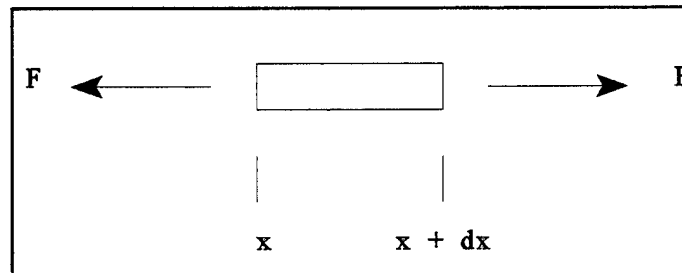


Figure 4.2. Differential Element of Rod

Next, consider that the cross-sectional area of the rod is uniform. Now, taking the derivative of both sides with respect to x gives:

$$\frac{dF}{dx} = 0 = EA \frac{d^2 u_{(x)}}{dx^2}. \quad (4.3)$$

Next, integrate to obtain:

$$u_{(x)} = c_1 x + c_2. \quad (4.4)$$

The time-dependant variables c_1 and c_2 are constants with respect to x .

The position of the rod at any given time (t) will be given by the displacement variable $u_{(x, t)}$. The position of the two nodes can then be expressed as:

$$\begin{aligned} u_1 &= u_{(0, t)} = u_1(t) \\ u_2 &= u_{(L, t)} = u_2(t) \end{aligned} \quad (4.5)$$

Substituting into Equation 4.4 gives:

$$u_1 = c_1(0) + c_2 = c_2 \quad (4.6)$$

and

$$u_2 = c_1 L + c_2. \quad (4.7)$$

Solving the simultaneous equations:

$$c_1 = \frac{u_2 - u_1}{L}; \quad c_2 = u_1 \quad (4.8)$$

and

$$u_{(x,t)} = \left(1 - \frac{x}{L}\right) u_1 + \left(\frac{x}{L}\right) u_2. \quad (4.9)$$

The coefficients of u_1 and u_2 are called the shape functions because they determine the spacial distribution, or shape, of the solution [Ref. 5:p. 140]. This leads to:

$$u_{(x,t)} = \alpha_{1(x)} u_1 + \alpha_{2(x)} u_2 \quad (4.10)$$

where the shape functions are:

$$\alpha_1 = 1 - \frac{x}{L}; \quad \alpha_2 = \frac{x}{L}. \quad (4.11)$$

The shape functions of any finite element are low order polynomials.

2. Determine Mass and Stiffness Matrices

Lagrange's method is used to obtain the element mass and stiffness matrices. In order to apply the Lagrangian equation, the internal kinetic energy and potential energy of

the rod must first be found. The internal strain (potential) energy (U) of a rod is found using [Ref. 8:p. 210]:

$$U = \int_V U_o dv; \quad U_o = \frac{1}{2E} \sigma_x^2 \quad (4.12)$$

where U_o is the strain energy density. Substitution yields:

$$U = \int_V \frac{E}{2} \left(\frac{\partial u}{\partial x} \right)^2 dv = \frac{AE}{2} \int_0^l \left(\frac{\partial u}{\partial x} \right)^2 dx. \quad (4.13)$$

The kinetic energy (T) is given by [Ref. 5:p. 404]:

$$T = \frac{1}{2} \int_0^l A_{(x)} \rho_{(x)} \left(\frac{\partial u}{\partial t} \right)^2 dx. \quad (4.14)$$

Now, if both the density and area are constant over the entire length:

$$T = \frac{\gamma}{2} \int_0^l \left(\frac{\partial u}{\partial t} \right)^2 dx \quad (4.15)$$

where the linear mass density (γ) is given by $\gamma = A\rho$. Substituting in Equation 4.10 and taking derivatives yields:

$$T = \frac{\gamma}{l} \int_0^l (\alpha_1 \dot{u}_1 + \alpha_2 \dot{u}_2)^2 dx \quad (4.16)$$

and

$$U = \frac{AE}{2} \int_0^l (\alpha'_1 u_1 + \alpha'_2 u_2)^2 dx. \quad (4.17)$$

Lagrange's equation is defined as [Ref. 5:p. 206]:

$$\frac{d}{dt} \left(\frac{\partial L}{\partial \dot{q}_i} \right) - \frac{\partial L}{\partial q_i} = 0, \quad i = 1, 2, 3, \dots \quad (4.18)$$

The Lagrangian operator (L) is defined as $L = T - V$ for continuous systems. The coordinates used are generalized coordinates. For this example $q_1 = u_1$ and $q_2 = u_2$.

Substituting Equations 4.16 and 4.17 into Lagrange's equation yields:

$$\begin{aligned} \gamma \int_0^l (\alpha_1 \ddot{u}_1 + \alpha_2 \ddot{u}_2) \alpha_1 dx - AE \int_0^l (\alpha'_1 u_1 + \alpha'_2 u_2) \alpha'_1 dx &= 0 \\ \gamma \int_0^l (\alpha_1 \ddot{u}_1 + \alpha_2 \ddot{u}_2) \alpha_2 dx - AE \int_0^l (\alpha'_1 u_1 + \alpha'_2 u_2) \alpha'_2 dx &= 0. \end{aligned} \quad (4.19)$$

These can be written as a system of equations:

$$\begin{bmatrix} \gamma \int_0^l \alpha_1^2 dx & \gamma \int_0^l \alpha_1 \alpha_2 dx \\ \gamma \int_0^l \alpha_1 \alpha_2 dx & \gamma \int_0^l \alpha_2^2 dx \end{bmatrix} \begin{Bmatrix} \ddot{u}_1 \\ \ddot{u}_2 \end{Bmatrix} - \begin{bmatrix} AE \int_0^l (\alpha'_1)^2 dx & AE \int_0^l \alpha'_1 \alpha'_2 dx \\ AE \int_0^l \alpha'_1 \alpha'_2 dx & AE \int_0^l (\alpha'_2)^2 dx \end{bmatrix} \begin{Bmatrix} u_1 \\ u_2 \end{Bmatrix} = \begin{Bmatrix} 0 \\ 0 \end{Bmatrix}. \quad (4.20)$$

For a system with constant γ , A and E, the mass elements are:

$$M_{ij} = \gamma \int_0^l \alpha_i \alpha_j dx \quad (4.21)$$

and the stiffness elements are:

$$K_{ij} = AE \int_0^l \alpha_i' \alpha_j' dx. \quad (4.22)$$

Solving for the rod gives:

$$M = \frac{\gamma l}{6} \begin{bmatrix} 2 & 1 \\ 1 & 2 \end{bmatrix}; \quad K = \frac{AE}{l} \begin{bmatrix} 1 & -1 \\ -1 & 1 \end{bmatrix}. \quad (4.23)$$

The matrices described by Equation 4.23 Are the elemental mass and stiffness matrices associated with a finite element of the bar described by Figure 4.1.

3. Modeling Multi-Element Structures

Finite element models are generally made up of many elements connected together. It is impractical, and unnecessary, to solve Lagrange's equations for these multi-element structures. Instead, the simple elements are used and superimposed upon each other to obtain the mass and stiffness matrices for the entire structure. Boundary conditions are then accounted for in order to obtain the final modal equation.

As an example, consider the cantilever rod shown in Figure 4.3. The rod is modeled using three finite elements with four nodes. Each element is of length $\frac{l}{3}$, so the mass and stiffness matrices become:

$$M = \frac{\gamma l}{18} \begin{bmatrix} 2 & 1 \\ 1 & 2 \end{bmatrix}; \quad K = \frac{3AE}{l} \begin{bmatrix} 1 & -1 \\ -1 & 1 \end{bmatrix}. \quad (4.24)$$

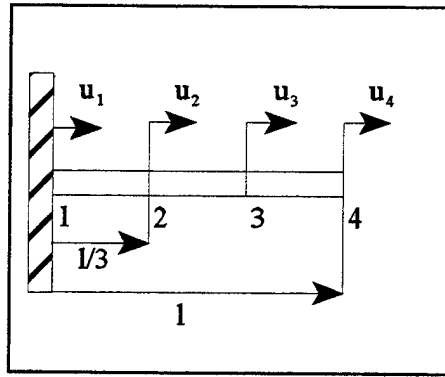


Figure 4.3. Cantilever Bar

Each of the three elements on the beam displaces two local coordinates. Using these coordinates, the equation of motion for the entire bar is written as a system of equations:

$$\frac{\gamma l}{18} \begin{bmatrix} 2 & 1 & 0 & 0 \\ 1 & 2+2 & 1 & 0 \\ 0 & 1 & 2+2 & 1 \\ 0 & 0 & 1 & 2 \end{bmatrix} \begin{Bmatrix} \ddot{u}_1 \\ \ddot{u}_2 \\ \ddot{u}_3 \\ \ddot{u}_4 \end{Bmatrix} + \frac{3AE}{l} \begin{bmatrix} 1 & -1 & 0 & 0 \\ -1 & 1+1 & -1 & 0 \\ 0 & -1 & 1+1 & -1 \\ 0 & 0 & -1 & 1 \end{bmatrix} \begin{Bmatrix} u_1 \\ u_2 \\ u_3 \\ u_4 \end{Bmatrix} = \begin{Bmatrix} 0 \\ 0 \\ 0 \\ 0 \end{Bmatrix} \quad (4.25)$$

The mass and stiffness matrices in Equation 4.25 are called the global mass and stiffness matrices. They are easily obtained by summing forces. Observe that the adjacent components of each elemental matrix are overlapped to form a diagonally banded global matrix.

The final procedure in creating a FEM is to account for any boundary conditions. This is done by eliminating the row and column in each matrix which is associated with the

restrained nodes. In Figure 4.3 the rod is clamped at node one. Therefore, row one and column one must be eliminated. The final global matrices become:

$$M = \frac{\gamma l}{18} \begin{bmatrix} 4 & 1 & 0 \\ 1 & 4 & 1 \\ 0 & 1 & 2 \end{bmatrix}; \quad K = \frac{3AE}{l} \begin{bmatrix} 2 & -1 & 0 \\ -1 & 2 & -1 \\ 0 & -1 & 1 \end{bmatrix}. \quad (4.26)$$

This procedure is used to combine many different elements together. The goal is to form a model which will accurately represent the motion of the actual system being considered. Specifically, for the vibration problem, the global matrices are used to solve the eigenvalue problem discussed in chapter three.

B. ASSOCIATED ERRORS

The process of modeling a continuous structure as a system of finite elements introduces errors when solving the vibration eigenvalue problem. There are several types of errors introduced. They arise during both the discretization of the structure and the interpolation of the element shape. There are also errors in the model stiffness associated with joints. Errors are also introduced when the modal solutions are truncated. While these are not associated with the finite element model itself, they inevitably appear when FEM solutions are truncated to match test data. This is done in order to allow the user to concentrate on those modes which are of primary importance.

During the discretization of the structure, the system is modeled as a collection, or mesh, of many finite elements. The elements are only an approximation of the true shape

of the structure. For instance, curved surfaces are modeled with straight elements. This is necessary in order to keep the equations of motion of the individual elements very simple. The response of the structure is then approximated by modeling the response at each of the nodes. The errors associated with these approximations can be minimized by increasing the number of elements.

Another level of approximation is introduced when estimating the response of the individual elements. The response of a finite element is determined by its associated shape function. For instance, the shape functions of a rod are shown in Figure 4.4. The shape functions are low order polynomials which are used to approximate the true shape. They satisfy the boundary conditions of the element, and they are integrable up to order of the strain energy [Ref. 6:p.252].

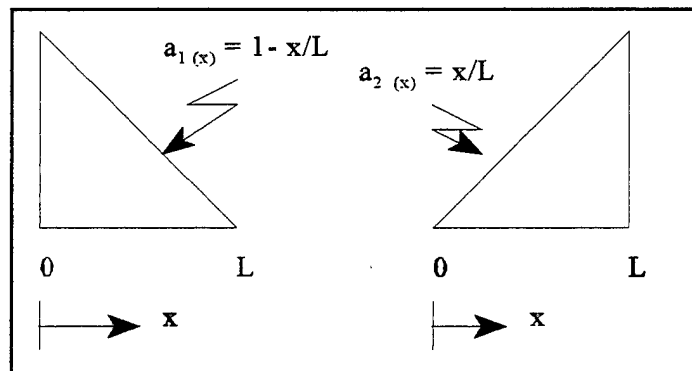


Figure 4.4. Shape Functions of a Simple Rod

In order to model the response of an element exactly under any load, a complex function is required. For instance, the exact analytic solution for the mode shape of the bar is given by [Ref. 5:p. 322] :

$$u = \cos \frac{n\pi x}{l}; n = 1, 2, 3, \dots \quad (4.27)$$

As can be seen from Equation 4.27, the lowest mode ($n=1$) is closely approximated by the polynomial solution shown in Figure 4.4. In order to solve for any higher modes, however, several elements would have to be used. Each element would show a linear response, but by connecting them together, the actual response would be approximated. From this analogy, it is seen that the more complicated responses (i.e., higher modes) have to be approximated with more elements. Said another way, given the same number of elements, the higher modes show a greater error.

Joints between structural elements are normally modeled with a node. There is not a stiffness associated with the joint. However, in the actual structure, the stiffness at a joint is different than that within the continuous member. The type of joint (e.g., welded, bolted, riveted) determines how the stiffness is affected. Normally, this does have a large impact on the overall response of a large structure. However, for those areas of the model which are considered critical, a point, or lumped, stiffness matrix can be added.

As previously mentioned, truncation errors are not associated with the mass and stiffness matrices obtained from the finite element method. They arise in when the large modal solutions of complicated structures are reduced in order to concentrate on the most important frequencies and mode shapes.

Consider a finite element structure subject to a forcing function,

$$[M]\{\ddot{q}\} + [K]\{q\} = [F] \quad (4.28)$$

The mass and stiffness matrices are each $[N \times N]$. There are, therefore, a maximum of N modes which can be determined. If only those modes under a certain frequency are to be considered, the model can be reduced to P modes. Not all of these modal frequencies are accurate, however. In order to determine the accuracy of a particular modal frequency (ω), the steady state solution to Equation 4.28 is evaluated.

If the structure is forced at frequency (Ω), the steady state modal solution becomes [Ref. 9]:

$$q_i = \frac{\frac{F_i}{K_i}}{1 - \left(\frac{\omega}{\Omega}\right)^2} \cos(\Omega t). \quad (4.29)$$

Transferring back to physical coordinates:

$$\{x_{(t)}\} = [\Phi]\{q_{(t)}\} = \sum_{i=1}^P \{\Phi^{(i)}\} q_{i(t)}; \quad P \leq N. \quad (4.30)$$

From Equation 4.30 it is seen that as more terms are included ($P \rightarrow N$), the solution becomes more accurate.

In order to determine how many terms are required, the contribution from the higher order terms to the total sum must be evaluated. The answer comes from analyzing

Equation 4.29. Of particular importance is the $\left(\frac{\Omega}{\omega_i}\right)^2$ term. If the forcing frequency approaches a particular modal frequency, then that term becomes important. Therefore, in order to obtain an accurate solution, modes up to the value of the forcing frequency must be considered. The normal practice is to include modes up to twice the forcing frequency.

V. THE OH-6A FINITE ELEMENT MODEL

At the outset of this project, it was desired to obtain an older NASTRAN finite element model of the OH-6A which had been produced by The McDonnell Douglas Helicopter Company for NASA [Ref. 2]. This model would have then been modified to match the test platform. After consultation with Dr. Mostafa Toossi at MDHC, it was determined that the OH-6A FEM was not available. However, MDHC was able to provide a somewhat more sophisticated model of a similar aircraft. This baseline model required some extensive modifications to both the nose and empennage in order to match the test platform.

A finite element model consists of both a stiffness model and a mass model. Together, these create the total dynamic model which can then be used to predict the actual response of the system. Typically, the FEM is developed using blueprints and other design information. However, the data was not available for this project. The absence of accurate structural design and weight distribution data for the OH-6A created some unique challenges in developing the FEM.

A. STRUCTURAL MODEL

In order to gain familiarity with the baseline model, initial research was completed at the MDHC facilities in Mesa, AZ over a two day period. With the help of John Fong, an intern Master's degree student from The California Polytechnic State University at San

Louis Obispo, the nose section was modified to closely match the test platform. In addition, preliminary research was done in order to help determine the internal structural components of the empennage. This work was extremely helpful in developing the OH-6A FEM seen in Figure 5.1.

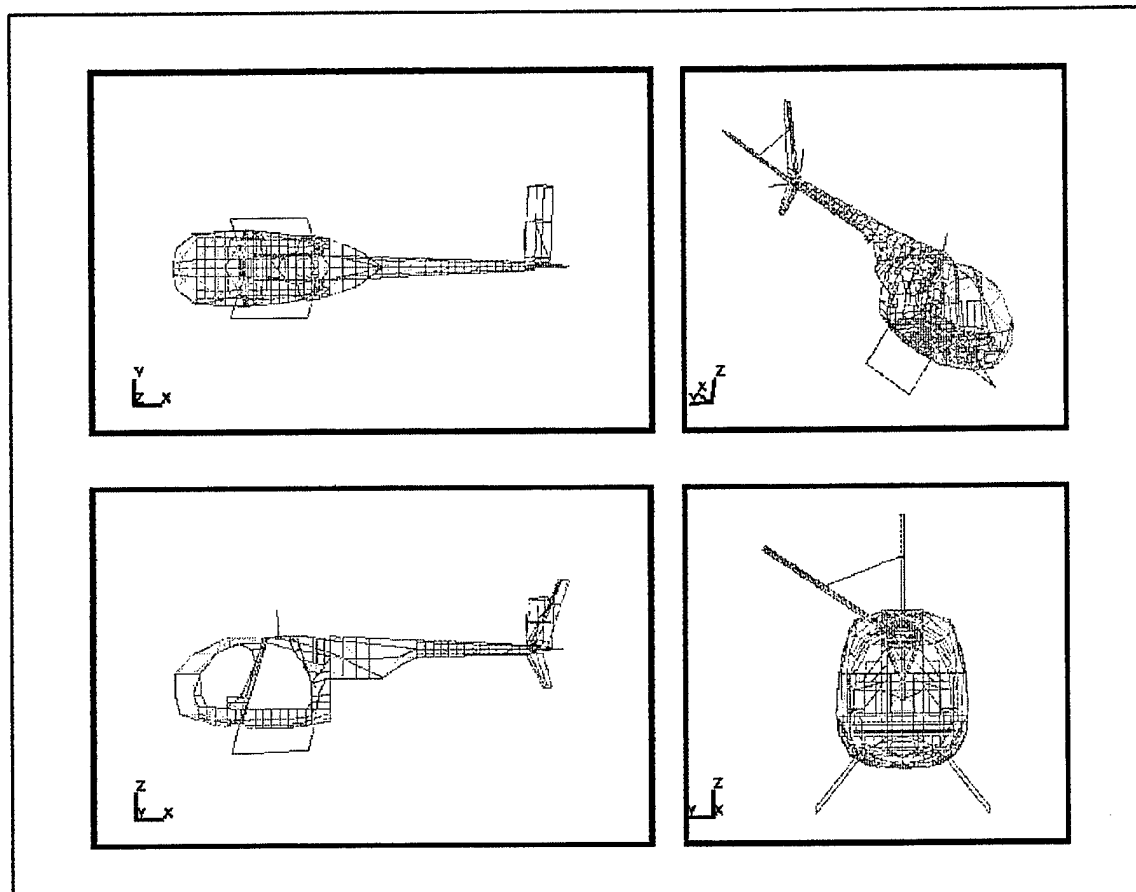


Figure 5.1. OH-6A Finite Element Model

1. Nose Section

The nose section of the baseline model was somewhat more elongated than that of the OH-6A. In order to reshape the nose, aircraft geometry had to be determined. The absence of accurate structural data made this exercise somewhat challenging.

The stations along the fuselage were determined using data contained in the OH-6A maintenance manual [Ref. 1] shown in Figure 5.2. Estimates of the shape were then

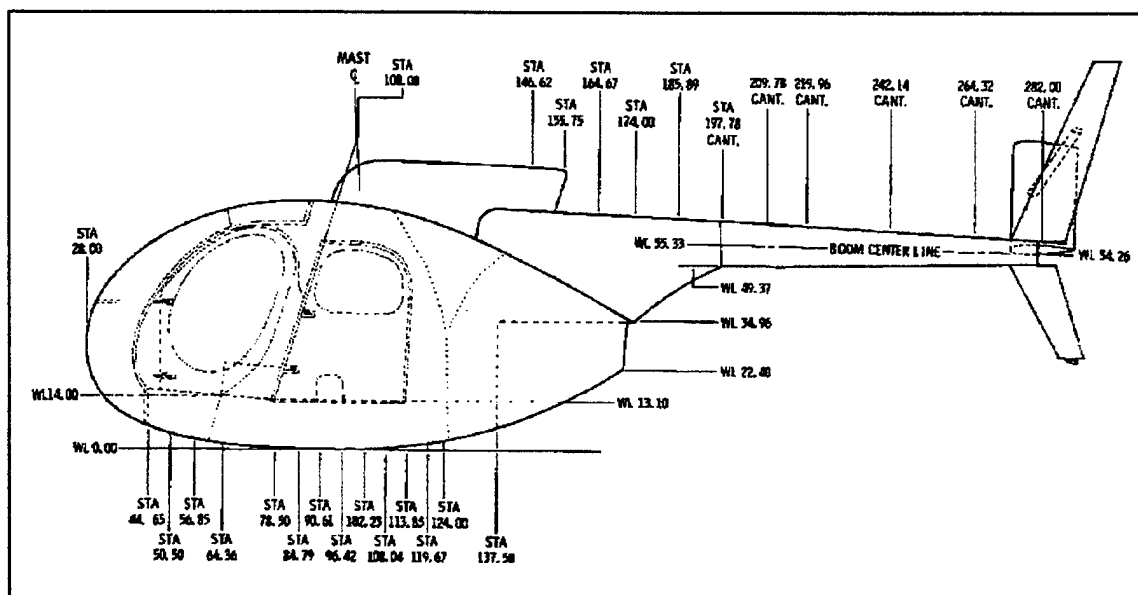


Figure 5.2. Location of OH-6A Stations. From Ref. [1].

made based on the length and visual inspection of the nose. Since the fuselage of the baseline model was similar to the OH-6A, its structure was not modified. In the nose area, grid points 3504 and 3510 were removed along with several elements which are shown in Table 5.1. Additionally, grid points 3506 and 3508 were moved aft to station 28.0. This give the model a rounder nose typical of the OH-6A.

Element Type	Elements Removed
CBAR	20507 - 20510
CQUAD4	4060444107, 4060544107, 4060644107, 4060744107, 4060844107, 4060944107,
CTRIA3	3017644107, 3017844107, 3018044107, 3018244107

Table 5.1. Removed FEM Nose Elements

2. Empennage Section

Tail modifications were much more extensive than the other sections of the aircraft. In order to accurately model the test platform, the entire empennage had to be replaced. In order to perform the necessary revisions without structural data the external geometry and the internal structural components had to be determined.

The empennage is shown in Figure 5.3. The first step in developing the model was to accurately determine external geometry. The OH-6A empennage consists of three airfoils connected to the end of the tailboom. Two of these, the vertical stabilizers, are vertically mounted to the top and bottom of the tailboom respectfully. The horizontal stabilizer is mounted on the starboard side of the tailboom at an angle of approximately 40 degrees off vertical.

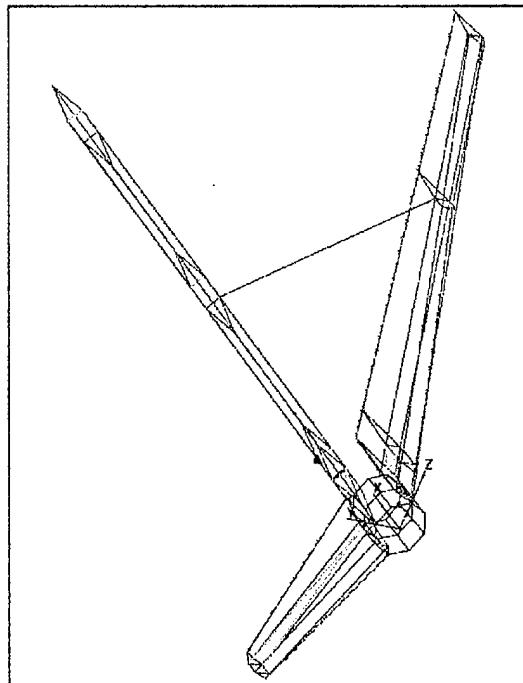


Figure 5.3. OH-6A Empennage

Measurements were taken of the test platform at NPS. The vertical and horizontal stabilizers were measured with reference to the tailboom. Cross-sectional depth was measured at the endpoints and determined by inspection to be uniform along the length of each of the stabilizers. The horizontal stabilizer was determined to be of constant cross-sectional area., while the vertical stabilizers are tapered toward the tips.

The FEM was modified using obtained measurements. All of the previous empennage elements were removed. These are given in Table 5.2 along with the modified element identification numbers. The corrected grid points and structural elements are given in Appendix E as NASTRAN formatted text. A new coordinate system was defined

as well. It is oriented orthogonally on grid point 27300 which is in the center of the tailboom directly below the connection point of the upper vertical stabilizer.

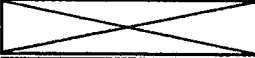
	Upper Vertical Stab.	Horizontal Stab.
Old Grid Points	31002 - 31088	32002 - 32108
New Grid Points	31018 - 31088	32002 - 32048

Table 5.2. Modified FEM Element Identification Numbers

Connection points for each of the stabilizers are modeled as rigid elements. Two elements are used at the base of each airfoil. The airfoil connection grid points and the corresponding connection points on the tailboom are given in Table 5.3 along with the rigid element identification numbers. Note that rigid elements 50003 to 50010 in the original model were deleted.


	Upper Vertical Stab		Lower Vertical Stab		Horizontal Stab	
Empennage G.P.	31008	31025	31073	31066	32002	32005
Tailboom G.P	27302	28002	28010	27310	27306	28006
Rigid Element ID.	50003	50004	50005	50006	50007	50008

Table 5.3. Empennage Connection Points

A first attempt was made to connect the lower vertical stabilizer at a single point on the tailboom. This approach matches the physical configuration. After calculating the normal modes of this model, however, it was determined that the first lateral, vertical and

torsional frequencies were incorrect. Also, there were two additional rigid body modes. Inspection of the mode shapes revealed that the lower stabilizer was vibrating independently of the rest of the empennage. This is not typical of the actual aircraft. The addition of another rigid element connection brought the frequencies and mode shapes closer to the test results.

Determination of the internal geometry was accomplished by measuring the location of rivet lines. Using this data, the location of the internal structural components was determined. Each of the airfoils is comprised of spars with spar caps running longitudinally with respect to the base. They are intersected by ribs which are oriented parallel to the base. Each end is comprised of a sheet metal cap reinforced with a rib. The top vertical and horizontal stabilizer are connected externally with a hollow sheet metal bar. The element identification numbers which were deleted from the original model as well as the new element numbers are given in Table 5.4.

Element	Original ID	New ID
CROD	10403 - 10407	10403 - 10450
CSHEAR	40483 - 40597	40483 - 40546
CBAR	20403 - 20478	20403 - 20469
CTRIA3	30124 - 30159	30124 - 30152
CQUAD4	40557	None

Table 5.4. FEM Element Identification Numbers

3. Structural Elements

While developing the FEM, assumptions had to be made concerning the types of internal elements to be used. Upon receiving the baseline model, the first operation performed was to calculate the natural frequencies and mode shapes. The frequencies from this model were close to that of the test platform. It was determined from this data and consultation with MDHC engineers that the material properties of the NPS test vehicle could be closely approximated using the material properties in the baseline model.

There were four different types of finite elements used in the construction of the tail model. These are summarized in Table 5.5. The spars were modeled using rod elements. Two sets of two longitudinal spars run the length of each airfoil. Each set has elements running along the top and bottom of the stabilizer. Between them is a flange or

Table 5.5. OH-6A Structural Components. After Ref. [2].

Component	Element
Spar	Rod Element
Skin	Shear Panel Element
Spar Cap	Shear Panel Element
Sheet Metal Rib	Bar Element
Connection	Rigid Element

spar cap. This is represented with a shear panel. The ribs are modeled using bar elements. Each end cap is modeled using shear panels to represent sheet metal. They are reinforced

with bar elements. Aircraft skin is modeled with shear elements covering the entire structure. As mentioned previously, the connections to the tailboom are represented with rigid elements.

All of the elements were modeled using the MAT1 card number one in the NASTRAN model. This corresponds to aluminum with a modules of elasticity of 10.6×10^6 psi., Poisson's ratio of 0.33 and unit weight of 0.120 lb/in^3 . The elements were given various dimensions which were based on data obtained from the original FEM. These element properties as well as the corresponding property identification numbers are given in Table 5.6.

a. Rod Element

The simplest element to define is the rod element. It is shown in Figure 5.4. Rod elements carry axial loads only. The rod is assumed to be cylindrical in shape for mathematical calculations. However, the actual elements modeled do not necessarily have to be cylindrical. Rods are connected at the two end points only. They may be used to model an element of variable cross section. To do that, however, several rods must be used, each with a different area. Since the rod elements do not carry any bending loads, they are used in conjunction with shear panels in the tail section. Shear panels placed between two rods accurately model the flanged spars in each airfoil.

Table 5.6. FEM Material Properties

Vertical Stabilizers								
	PROD		PSHEAR		PSHELL		PBAR	
	PID	Diam.	PID	Thick	PID	Thick	PID	Width
Fwd Spar	11030	0.030	14040	0.040				
	11036	0.036	14048	0.048				
	11042	0.042	14055	0.055				
Aft Spar	11030	0.030	14040	0.040	13071	0.071		
	11044	0.044	14058	0.058				
	11057	0.057						
Ribs	11298	0.298					12014	0.014
End Caps			14025	0.025	13025	0.025	12017	0.017
Horizontal Stabilizer								
Spars	11030	0.030	14040	0.040				
End Caps	12067	0.067						
	12177	0.177						
Connecting Bar							12122	0.122

b. Bar Element

A bar element defines a simple beam. These elements carry bending as well as axial loads. The cross section of the bar is square with uniform area as seen in Figure 5.5. As with the rod, the material properties of each element are invariant throughout the

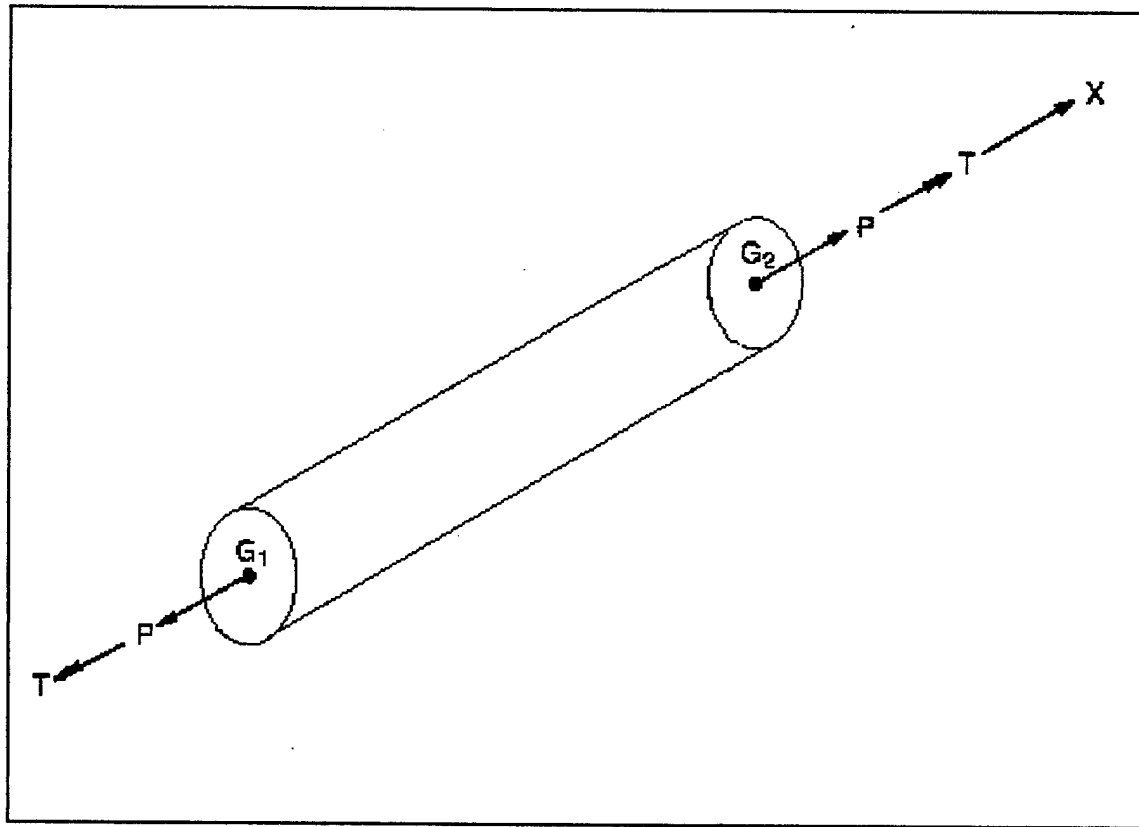


Figure 5.4. Rod Element. From Ref. [10].

entire length. In order to model a variable cross-section area, several bars connected together must be used. An alternate approach is to use a more sophisticated beam element; however, they are not used in this model. Bar elements are oriented using an orientation vector as shown in Figure 5.5. The vector is defined from node GA to grid point GO. The bar elements in this model are used to represent sheet metal ribs internal to each airfoil.

c. Shear Panel Element

Shear panel elements define a thin shell. The shell is a two dimensional solid with small thickness as compared to the length and width [Ref. 10:p. 175]. The shape of the shear panel is defined by the location of its four grid points as shown in Figure 5.6. It is noted that interior angles must be less than 180 degrees. Also, element thickness is defined as constant throughout the entire element.

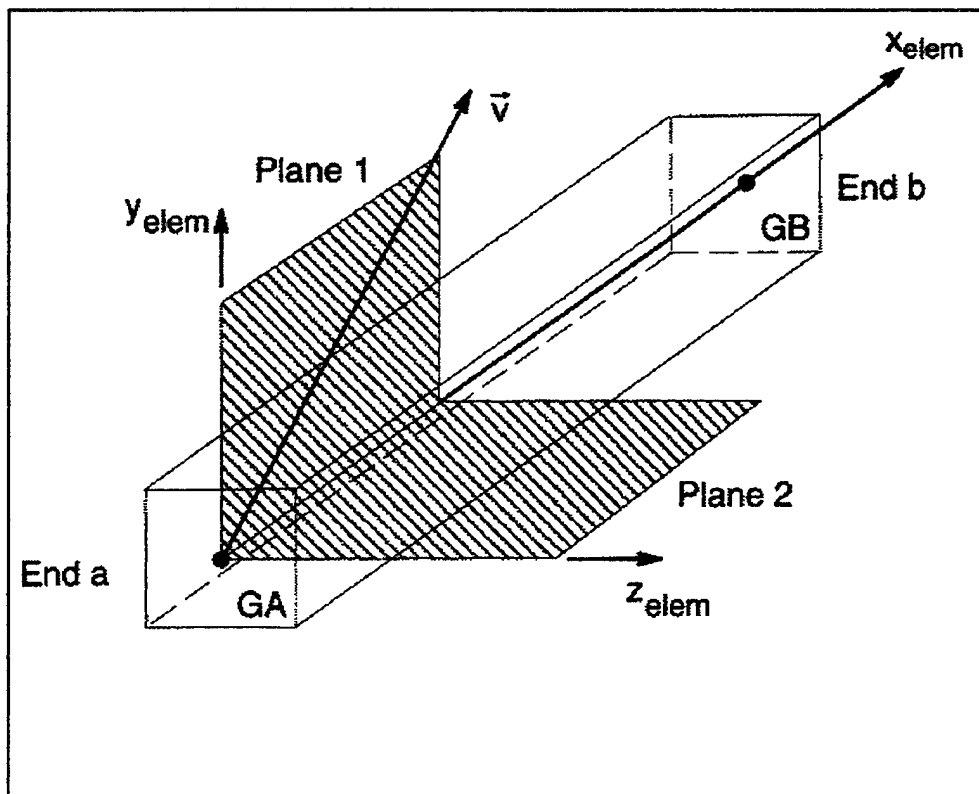


Figure 5.5. Bar Element. From Ref. [10].

Shear panels carry both shear and axial loads. They are used to model the aircraft skin which is a uniform thickness over the entire airfoil. As mentioned previously, they are also used in conjunction with rod elements to model spar caps.

d. Rigid Elements

A rigid element defines a rigid beam with six degrees of freedom at each end. The beam is massless with infinite stiffness. The degrees of freedom are defined as being either dependant or independent at each node. The rigid bar does not deform. It transfers the loads applied at the independent node to the dependant node in each DOF. Rigid elements are used at the base of each of the stabilizers. All six of the independent DOF are connected to the tailboom for each of the elements. The dependant DOF are at the nodes connected to the stabilizers.

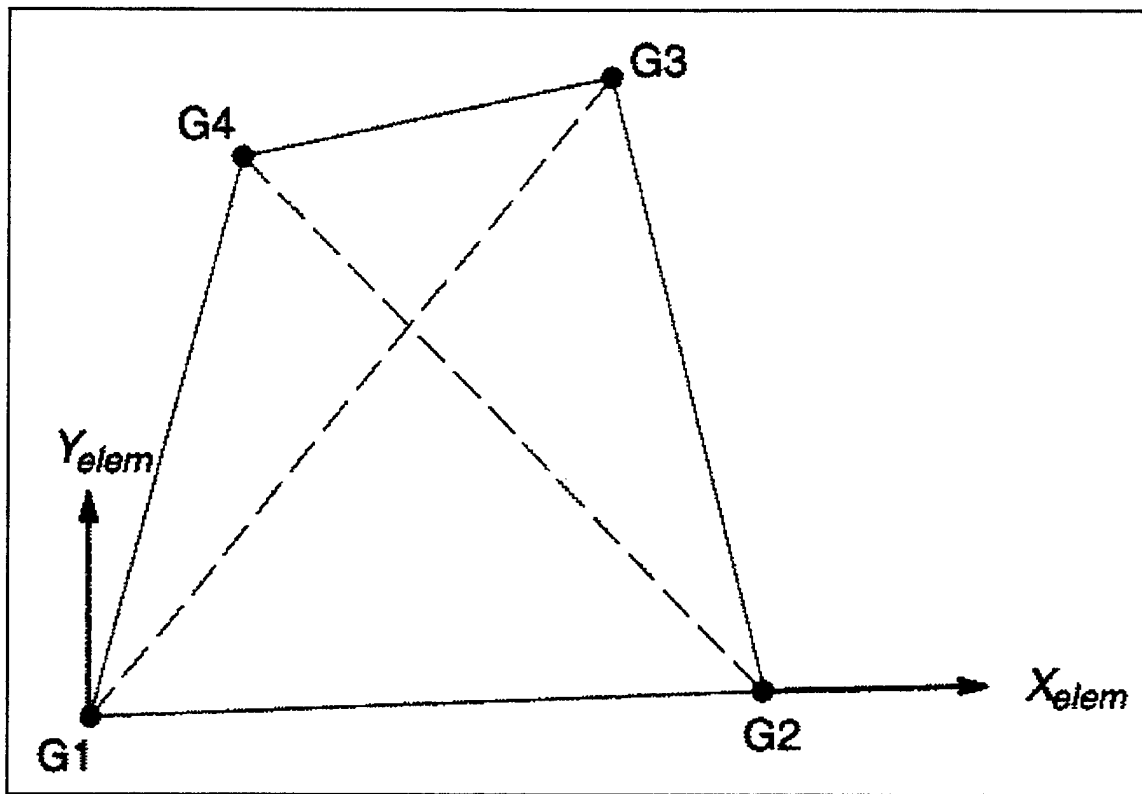


Figure 5.6. Shear Panel Element. From Ref. [10].

B. MASS MODEL

In addition to the structural model, the typical FEM includes a mass model as well.

The mass model of the OH-6A includes non-structural mass and structural mass. The non-structural mass includes the fuel crew and cargo weights. In this model, these were set to match the test configuration [Ref. 3]. This is shown in Table 5.7.

Table 5.7. OH-6A NPS Vibration Test Configuration. After Ref. [3].

Item	Weight (lbs.)	Fuselage Station
Ship as Weighed	1299	105.1
Crew	0	
Fuel	12	102.23
Additional Ballast	80	105.1
Total/C.G Station	1391	105.1

Structural masses are classified into two categories. Primary structural masses are determined from the mass densities of each of the elements of the model. Secondary structural masses are items such as equipment and useful load items [Ref. 2:p. 36]. These items are things such as rotor blades, engines, transmission components, etc. They are normally determined using blueprints and the associated weight report. The masses can be placed on the structure manually or by using an automated mass distribution program.

Without detailed structural data it was not possible to determine the secondary masses and their location on the empennage. In order to complete the dynamic model, a design sensitivity approach was taken. Using this method, the response of the structure to small changes in mass is calculated. Using the obtained sensitivity information, the change in mass required to produce the desired response is then determined.

In order to use the design sensitivity approach, the response of the system without mass must first be determined. This was done for the OH-6A model after the completion

of the structural model. The frequencies for each of the modes of interest is noted in Table 5.8.

The standard approach using design sensitivities is to place lumped masses at several points on the structure in order to obtain the total response. For this model, however, it was not necessary. As seen in Table 5.8, the model is very accurate even prior to the addition of any mass. With this information, it was determined that a single mass located near the center of mass of the empennage section would be sufficient. The mass was given both translational and rotational components. This corrected for the spacial distribution of the actual mass of the system.

Design sensitivities are determined from placing small masses at selected points of the structure and measuring the response. Consider the small component of mass, δM_j , placed at the selected point. The natural frequencies of the structure with this mass applied are given by $\{\omega\}_\delta$. If the natural frequencies of the model prior to the addition of the small mass are given by $\{\omega\}_a$, then the sensitivity matrix is defined by:

$$S_{i,j} = \frac{(\omega_i)_a^2 - (\omega_i)_\delta^2}{\delta M_j}. \quad (5.1)$$

This gives the sensitivity of the frequency components to a change in mass.

Table 5.8. Natural Frequencies Prior to Mass Model

Mode	Test Frequency (Hz)	Base Anal. Freq. (Hz)
1 st Lateral	9.32	9.01
1 st Vertical	9.97	9.01
1 st Torsional	15.01	15.42
Aft Vertical	15.61	15.84
2 nd Vertical	21.83	19.86
2 nd Lateral	27.48	26.80

The natural frequencies of the test platform are then compared to the base analysis frequencies:

$$\Delta\omega_i^2 = (\omega_i)_a^2 - (\omega_i)_T^2 \quad (5.2)$$

where $(\omega_i)_T$ are the test frequencies of interest. In order to solve for the mass, the sensitivity matrix is then applied to the frequencies. This is given as:

$$\{\Delta\omega^2\} = [S]\{\Delta M\}. \quad (5.3)$$

This equation can be solved to determine the change in mass, $\{\Delta M\}$, required to produce the desired change in frequency. It should be noted that the above calculations were

completed using units of force not mass. The force components are entered into NASTRAN which then converts them to mass.

After application of the sensitivity matrix, the determined mass was applied to the empennage. The mass matrix is shown in Table 5.9. Table 5.10 gives the model mass summary.

Table 5.9. Tail Force Components

Force Component	Magnitude
M_x	38.0 lb.
M_y	38.0 lb.
M_z	38.0 lb.
I_{xx}	100.0 in.-lb.
I_{yy}	524.0 in.-lb.
I_{zz}	600.0 in.-lb.

Table 5.10. OH-6A FEM Mass Summary

Component	Weight (lbs.)	Fuselage Station
Structural Weight	1375.55	114.83
Fuel	12	102.23
Crew	0	
Total Weight/C.G Location	1387.55	114.83

The first calculation using this method did not produce favorable results. A determination was made that the original point of application was not satisfactory, and a

new location was chosen. This position proved to be ideal. It is located on the bottom of the horizontal stabilizer just outboard of the tailboom at grid point 32022. It can be seen as a triangular mark in Figure 5.3. The NASTRAN force components used in the FEM are included at the end of Appendix E.

VI. COMPARISON OF RESULTS

Verification of a finite element model requires comparison of the analytical natural frequencies and mode shapes with an experimental vibration test. This finite model, however, was created using the previously generated test frequencies. By definition, therefore, they are closely correlated after completion of the completion of the mass modeling as shown in Table 6.1. The only exercise which remains is to compare the mode

Table 6.1. Natural Frequencies of Dynamic OH-6A FEM.

Mode	Test Frequency (Hz)	Analysis Freq. (Hz)	% Error
1 st Lateral	9.32	9.32	0.0%
1 st Vertical	9.97	9.99	0.2%
1 st Torsional	15.01	15.40	2.6%
Aft Vertical	15.61	15.82	1.3%
2 nd Vertical	21.83	19.84	9.1%
2 nd Lateral	27.48	26.79	2.5%

shapes. This will determine if the modes are matched.

A. MODAL ASSURANCE CRITERION

There are several methods which can be used to compare experimental and analytical mode shapes. These include both graphical as well as mathematical techniques.

For this thesis, a mathematical approach called Modal Assurance Criterion (MAC) was used. This and other mathematical modal parameters are based on graphical techniques. Therefore, before discussing the mathematical approach, some insight into the graphical method is necessary.

Graphical comparison of mode shapes is relatively straight forward. The simplest procedure is to place one mode shape on top of the other and visually compare deviation. Although this method is uncomplicated to perform, it has the disadvantage that the deviations are somewhat difficult to interpret [Ref. 11:p. 222]. A more sophisticated approach is to make a plot of the experimental modal deviation vs. the analytical deviation. This plot is shown in Figure 6.1.

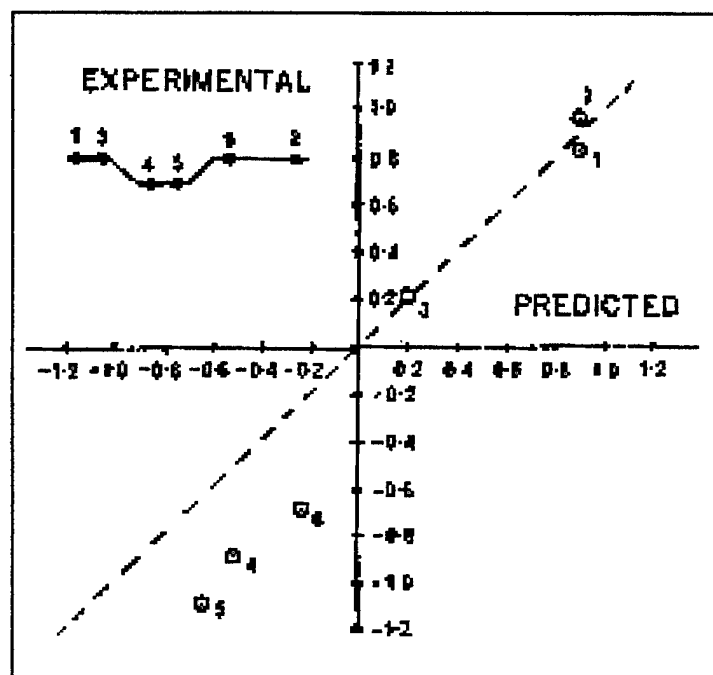


Figure 6.1. Mode Shape Comparison. From Ref. [11].

The predicted response is plotted along the abscissa with the experimental response on the ordinate. The resulting points should be disbursed about a 45 degree line as shown. It should be noted at this point that two assumptions are made when plotting these points:

1. Mode shapes must be identically normalized
2. Mode shapes must be plotted at identical points on the structure.

Deviations from the straight line can then be interpreted. For instance, a systematic deviation which produces a straight line offset from the origin may indicate a problem with the material properties of the model. A deviation which produces a straight line other than 45 degrees through the origin may indicate a problem with the experimental observations, perhaps an incorrect scaling of the FRF plots [Ref. 11:p. 223].

Mathematical calculations generally produce statistical properties of the deviation of the graphical solution from an ideal 45 degrees. The benefit of the MAC parameter is that it produces a least squares deviation from a straight line correlation. This allows the user to determine the quality of the fit of the analytical mode shape. This is not available with other approaches [Ref. 11:p.225].

In this thesis there are two mode shape matrices that are to be compared, the experimentally derived mode shape $[\Phi^*]$ and the analytically produced mode shape, $[\Phi^a]$. The MAC matrix is defined as:

$$MAC = \frac{([\Phi^x]^T [\Phi^a])^2}{([\Phi^x]^T [\Phi^x])([\Phi^a]^T [\Phi^a])} \quad (6.1)$$

The MAC matrix is square with the rows representing the experimental modes and the columns representing the analytical modes. If any two modes correlate exactly, the MAC will be unity for that position in the matrix. If there is no correlation, the MAC will be zero. For example, two perfectly correlated [3x3] mode shapes will give:

$$MAC = \begin{bmatrix} 1 & 0 & 0 \\ 0 & 1 & 0 \\ 0 & 0 & 1 \end{bmatrix} \quad (6.2)$$

Also, if the two modes differ only by a scalar, the scalars will divide out in Equation 6.1, and the MAC will be the same. Therefore, the MAC is independent of the normalizing constant of each particular mode shape.

In practice, the correlation won't be exactly unity or zero. It is generally accepted that a MAC greater than 0.9 indicates a correlated mode. A MAC less than 0.05 indicates uncorrelated data [Ref. 11:p. 226].

B. MATRIX REDUCTION

As indicated in the previous section, in order to perform mode shape comparison, the two mode shapes must be determined from identical points on the structure. In most

cases, however, the experimental data is determined from fewer points than the analytical data. In this thesis the test set consisted of between 17 and 20 points, depending on the mode. The analysis set, however, contained over 3000 nodes. In order to compare the two shapes, the analysis set must be reduced.

The reduction of the analysis response matrix is accomplished using a transformation matrix [T]. This is applied to the full element model, resulting in a test analysis model (TAM). The TAM matches the nodes in the experimental set [Ref. 12:p. 270]. It can then be solved for the modes of interest and compared to the experimental data set using the techniques described in the previous section.

The simplest reduction is a static reduction of the model. This is accomplished by first determining which DOF are to be kept in the TAM. Assuming an omitted set (o) and a retained set (a), the full model can be partitioned as:

$$\begin{bmatrix} M_{aa} & M_{ao} \\ M_{oa} & M_{oo} \end{bmatrix} \begin{Bmatrix} \ddot{x}_a \\ \ddot{x}_o \end{Bmatrix} + \begin{bmatrix} K_{aa} & K_{ao} \\ K_{oa} & K_{oo} \end{bmatrix} \begin{Bmatrix} x_a \\ x_o \end{Bmatrix} = \begin{Bmatrix} 0 \\ 0 \end{Bmatrix} \quad (6.3)$$

If an [N x a] transformation matrix is assumed, then:

$$\begin{Bmatrix} x_a \\ x_o \end{Bmatrix} = [T] \{x_a\} \quad (6.4)$$

Equation 6.4, 6.12 may then be substituted into Equation 6.3. It is then pre-multiplied by $[T]^T$ to give:

Equation 6.4 may then be substituted into Equation 6.3. It is then pre-multiplied by $[T]^T$ to give:

$$[\tilde{M}]\{\ddot{x}_a\} + [\tilde{K}]\{x_a\} = 0, \quad (6.5)$$

with $[\tilde{M}] = [T]^T[M][T]$ and $[\tilde{K}] = [T]^T[K][T]$. The associated eigenvalue problem may then be solved to produce the TAM frequencies and mode shapes

$$[\tilde{K}]\{\Psi\}^i = \omega_i^2[\tilde{M}]\{\Psi\}^i. \quad (6.6)$$

This produces the $[a \times a]$ matrix of mode shapes $[\tilde{\Psi}]$ which correlates to the reduced set of natural frequencies.

In order to determine the transformation matrix $[T]$, the full partitioned model is again considered. If a harmonic solution to Equation 6.3 is considered, the equation of motion at a particular frequency (Ω) may be written as:

$$\left(\begin{bmatrix} k_{aa} & k_{ao} \\ k_{oa} & k_{oo} \end{bmatrix} - \Omega^2 \begin{bmatrix} m_{aa} & m_{ao} \\ m_{oa} & m_{oo} \end{bmatrix} \right) \begin{Bmatrix} x_a \\ x_o \end{Bmatrix} = 0. \quad (6.7)$$

The static transformation matrix is found assuming zero frequency. The omitted set can then be written as:

$$\{x_o\} = [k_{oo}^{-1}][k_{oa}]\{x_a\} \quad (6.8)$$

Substituting Equation 6.8 into Equation 6.4 gives:

$$\begin{Bmatrix} \{x_a\} \\ -[k_{oo}]^{-1}[k_{oa}]\{x_a\} \end{Bmatrix} = \begin{bmatrix} [I] \\ -[k_{oo}]^{-1}[k_{oa}] \end{bmatrix} \{x_a\} = [T]\{x_a\} \quad (6.9)$$

It follows, then, from Equation 6.9 that the static transformation matrix is:

$$[T] = \begin{bmatrix} [I] \\ -[k_{oo}]^{-1}[k_{oa}] \end{bmatrix} \quad (6.10)$$

Static reduction is the simplest method of reducing the analysis model to obtain a TAM of equivalent size to the experimental model. There are other methods. Gordis gives a discussion on the Improved Reduction System TAM which provides increased accuracy over the static TAM by including inertia forces [Ref. 12]. The reduced model for this thesis was generated by NASTRAN using the SET command. NASTRAN automatically calculates the TAM using the static reduction method.

C. COMPARISON PROCEDURES

In order to use data sets in NASTRAN, the experimental data points must be mapped to specific grid points on the model. In his shake test of the OH-6A, Harris positioned the accelerometers on known aircraft stations [Ref. 3:p.34]. Plots of the resulting mode shapes are reproduced in Appendix A. It must be noted, however, that separate measurement points were used for the vertical, lateral and torsional mode shape

measurements. Therefore, three separate grid point data sets were determined from the model for calculations in NASTRAN.

The mode shape output from NASTRAN can be sent to a text file called Output Four (.op4). It was desired for this project to use MATLAB to manipulate the mode shapes. In order to accomplish this, a short MATLAB function called *shapes.m* was created which reads the contents of the NASTRAN generated file and puts it in MATLAB format. This code is contained in Appendix B.

Once the mode shape matrix is obtained, the desired mode shape vectors must be extracted. The output from the MATLAB *shapes* function is in the form:

$$\Phi = [\{\phi_1\}\{\phi_2\}\{\phi_3\}\dots]. \quad (6.11)$$

Each mode shape vector in N DOF, where $N = (6)(\text{\#grid points})$. Each grid point has six DOF listed in order from the top of the vector as $x, y, z, \theta_1, \theta_2, \theta_3$. In order to obtain only the desired mode shape, first the entire mode shape vector must be extracted from the Φ matrix. Then, all the rows not desired must be removed. For example, for the lateral mode shapes only rows 2, 8, 14, ... are kept. The mode shapes extracted for each of the modes is given in MATLAB format in Appendix C.

A second MATLAB program was used to MAC the mode shapes together. This code was provided by Professor Josh Gordis and is given in Appendix D. The results of the MAC are shown in Table 6.2.

Table 6.2. MAC Parameters

Mode	MAC
1 st Lateral	0.704
1 st Vertical	0.921
1 st Torsional	0.633
Aft Vertical	N/A
2 nd Vertical	0.903
2 nd Lateral	0.544

D. MODE SHAPES

1. Lateral Modes

Correlations for the lateral modes were not as accurate as for the vertical modes. The first lateral mode is somewhat correlated. The mode shape is shown in Figure 6.2. It demonstrates a somewhat steeper curvature in the tailboom than the experimental mode shape. Harris found the nodes at stations 80 and 214. In the FEM, the nodes appear at approximately stations 100 and 225. The mode shape is very similar to a cantilever beam first bending mode. This is expected due to the relative flexibility of the tailboom relative to the fuselage.

The second lateral mode shape is seen in Figure 6.3. There appears to be significant error associated with this mode. The general shape of the modes are similar, but the analytical mode is shifted forward relative to the experimental mode shape. Also, the relative deflection appears to be smaller. The mode shape also shows some degree of

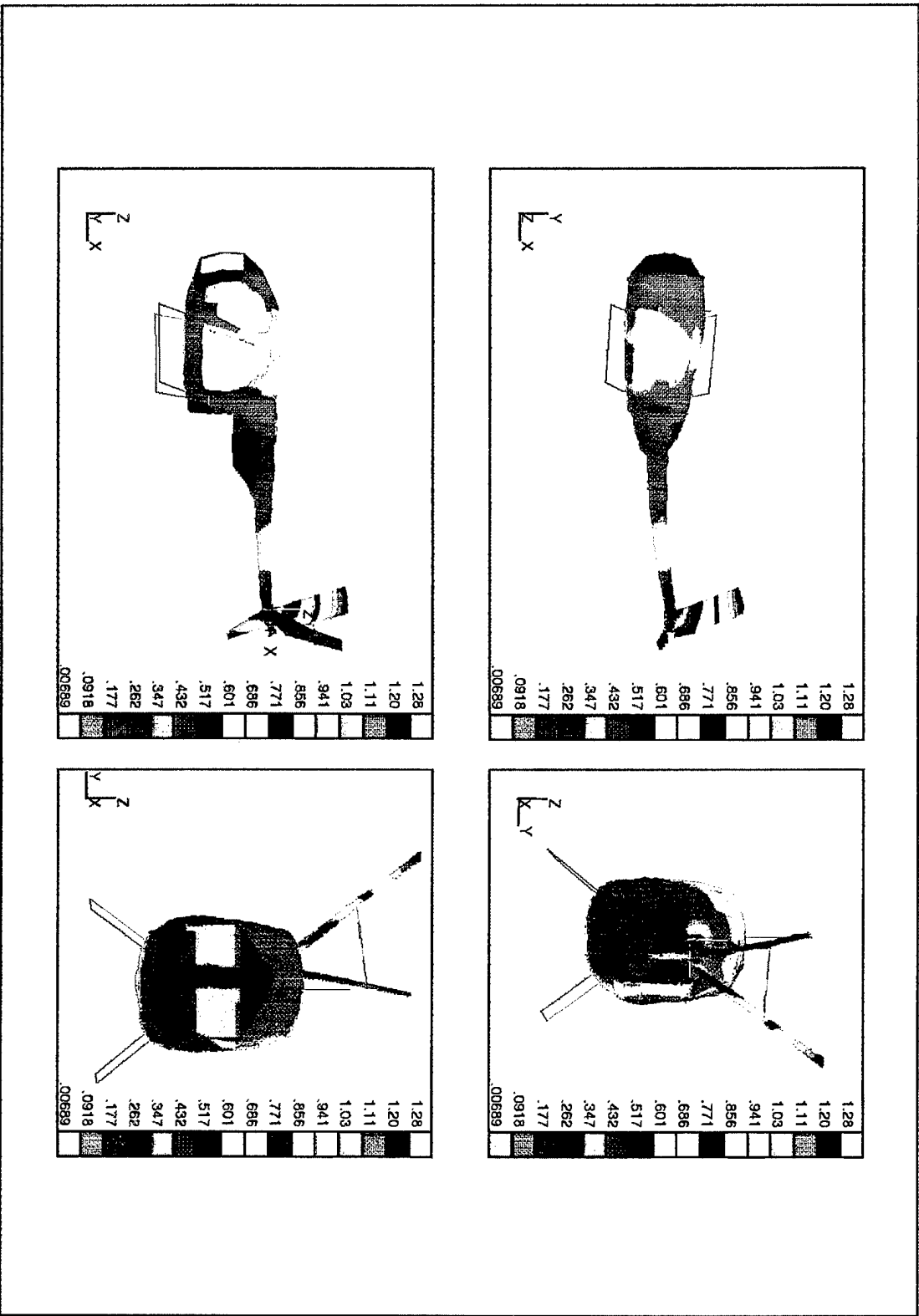


Figure 6.2. First Lateral Mode Shape at 9.32 Hz.

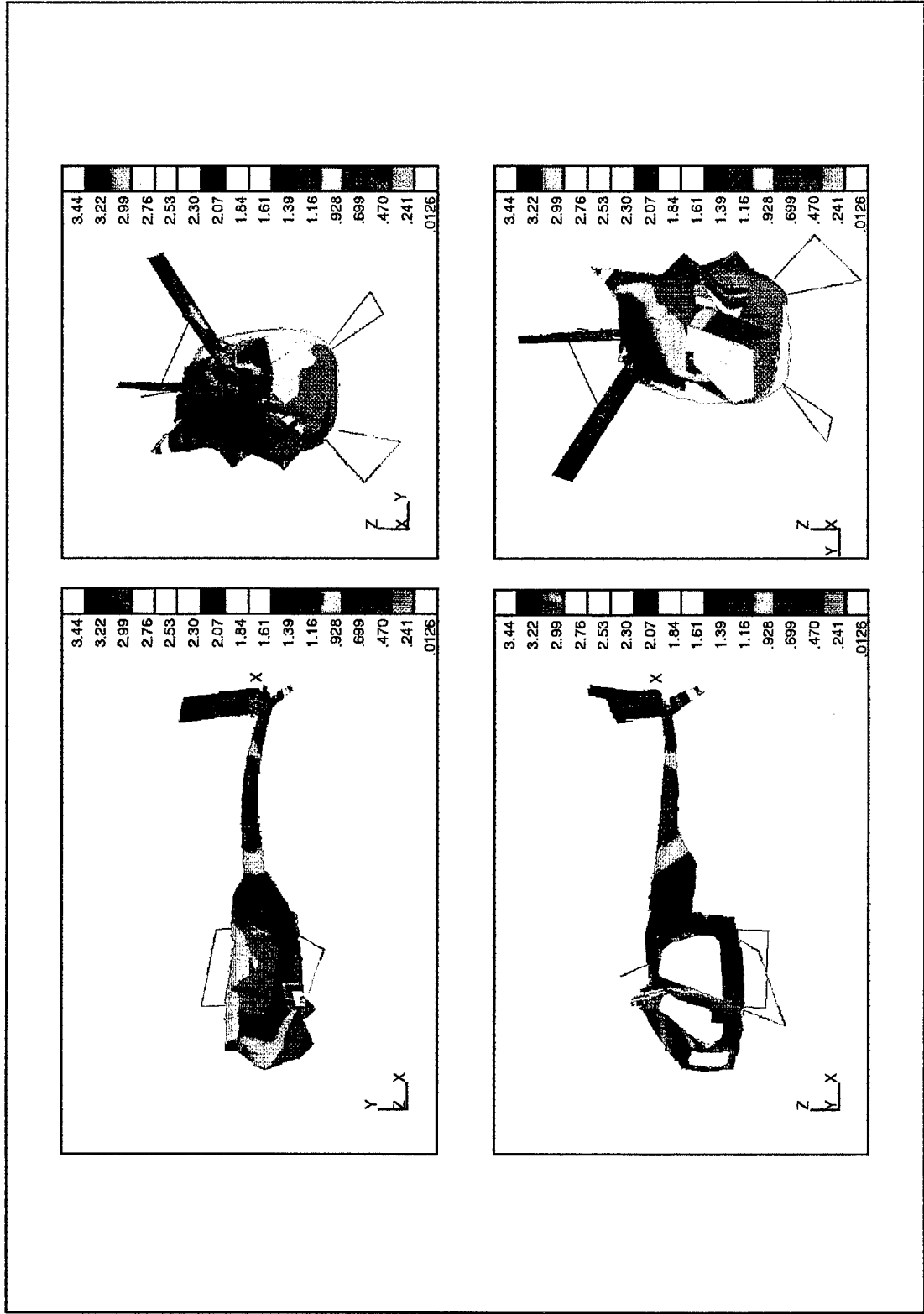


Figure 6.3. Second Lateral Mode Shape at 26.79 Hz.

coupling with the landing skids. Additionally, there are several points on the fuselage which appear to be excited at this frequency. It is possible that these components in the model are causing errors in the mode shape as well as the frequency solution.

2. Vertical Modes

The vertical mode shapes correlate very well with the experimental data. It is interesting to note that there is a degree of correlation between the first lateral and vertical mode shapes. The first vertical mode shape is seen in Figure 6.4. It appears to bend in much the same way as the lateral mode. This is typical of a cantilever beam. The bending mode shapes of a symmetrical beam (e.g., a circular tailboom) are ideally identical in both planes.

It is somewhat unexpected that the mode shapes of the second vertical modes correlate so well. The natural frequencies of the second vertical modes have the greatest discrepancy of all the modes. This mode shape, however, is simpler than the lateral mode as seen in Figure 6.5. It has more of a first mode shape with only two nodes. The less complicated shape makes it easier to model using a small number of points.

The aft vertical mode is shown in Figure 6.6. There was no data available for the experimental counterpart to this mode shape. Therefore, it does not have a MAC. The MDHC report on the OH-6A shake test [Ref. 2:p. 66] classifies this as an aft fuselage bending mode. The model mode shape generated for this report appears to display aft fuselage bending, but it is also coupled with a landing skid flapping mode.

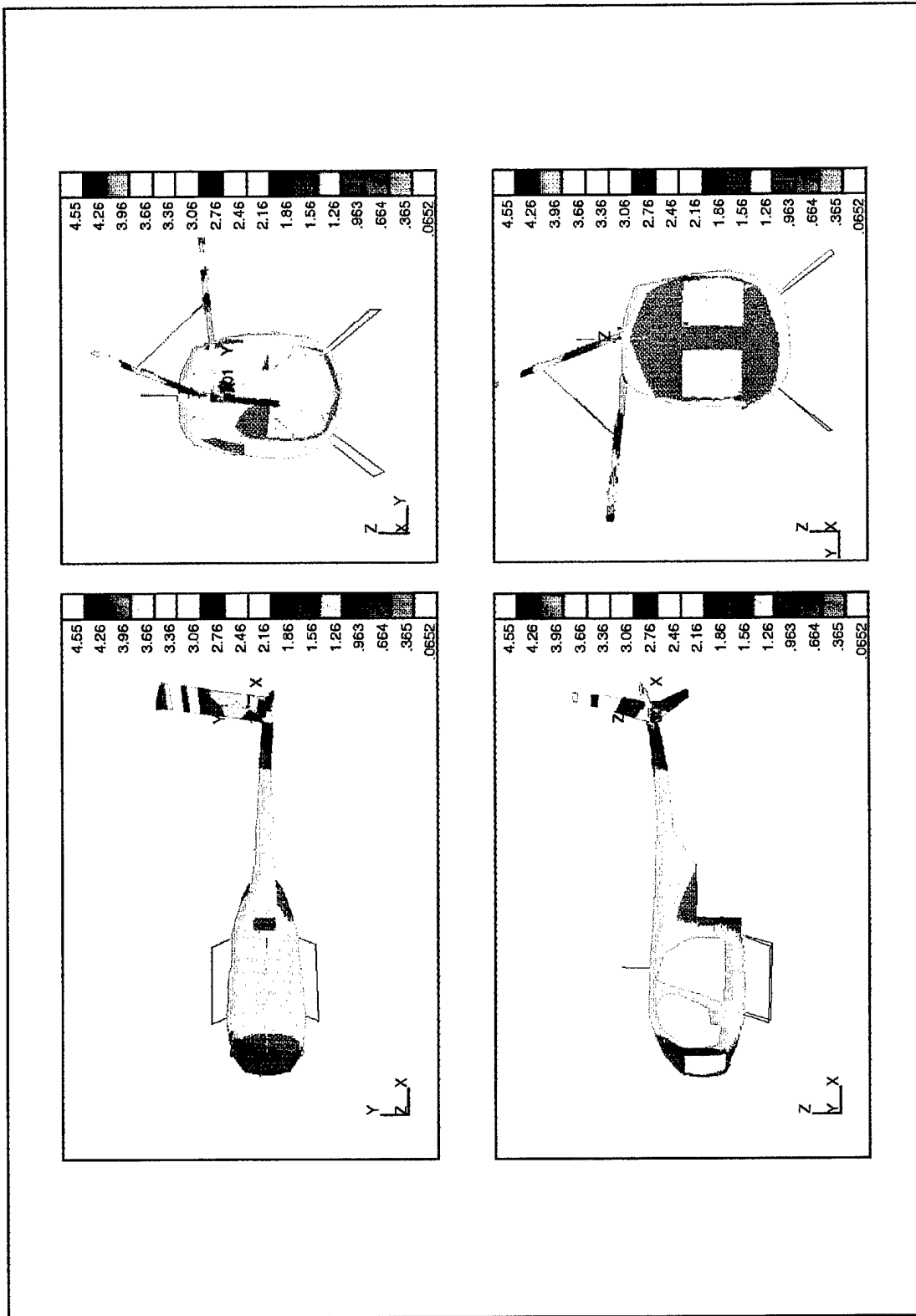


Figure 6.4. First Vertical Mode Shape at 9.99 Hz.

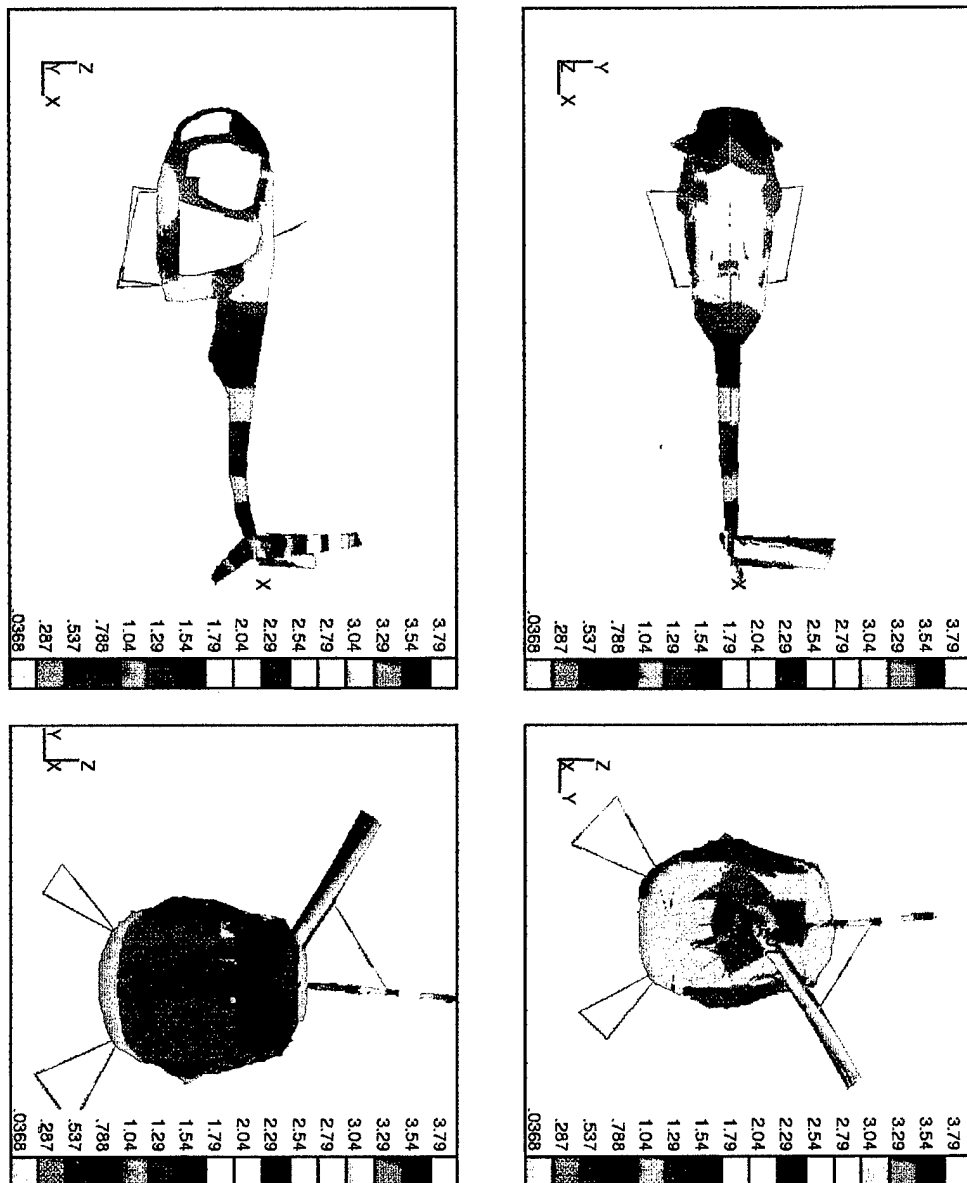


Figure 6.5. Second Vertical Mode Shape at 21.83 Hz.

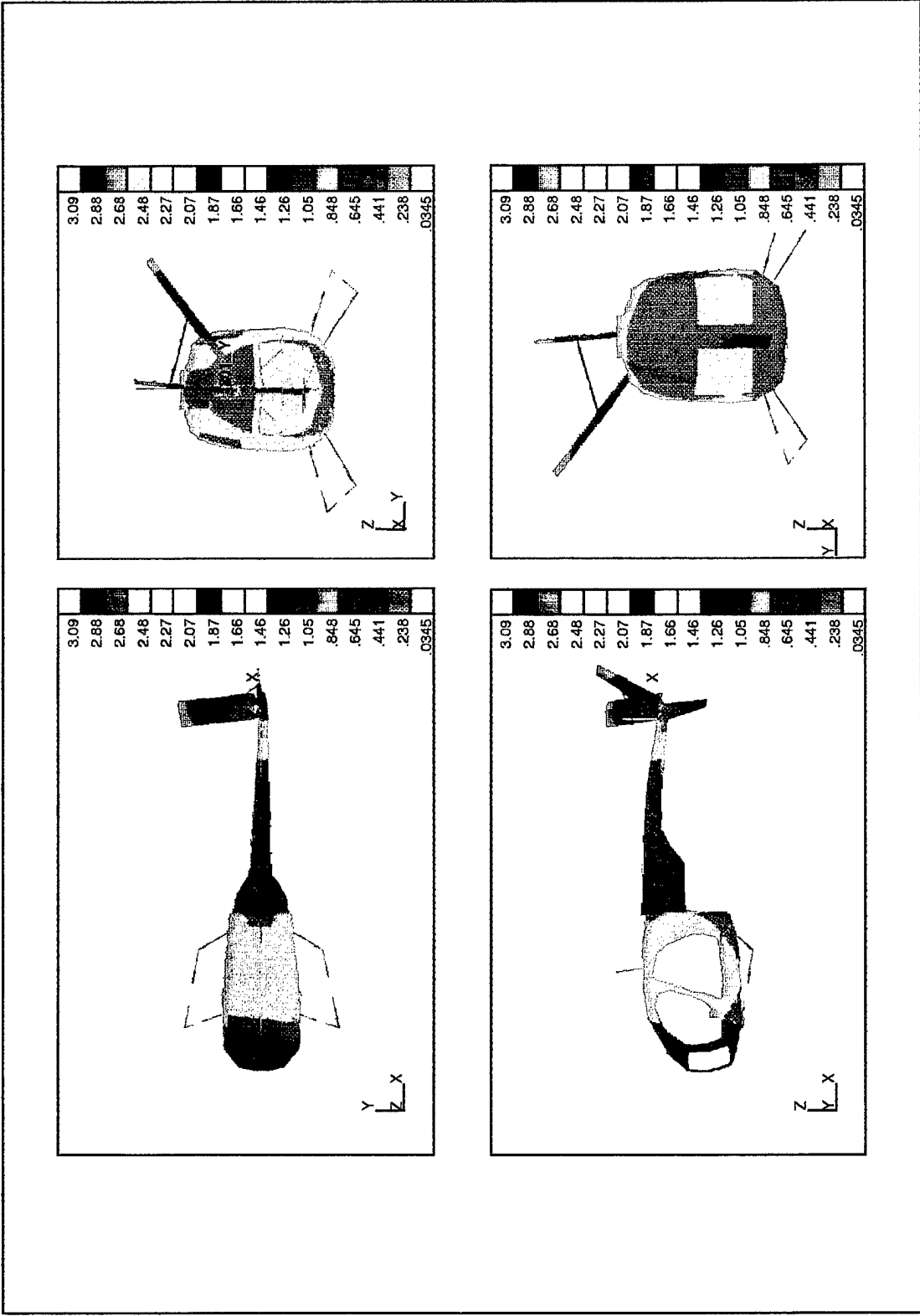


Figure 6.6. Aft Fuselage Vertical Mode Shape at 15.82 Hz.

3. Torsional Mode

The torsional mode shapes did not correlate well. Harris provided data for this mode, but there is no mode shape plot available from the experimental data. However, a visual inspection of Figure 6.7 shows similar deformation to the mode shape calculated by MDHC [Ref. 2:p. 61]. There were significant sources of error in correlating these plots. Only eight data points were used to correlate data. There were a total of 12 points in the test, but only eight were used because the others were not represented as grid points on the model. Also, only vertical deflections were measured. To get a more accurate measure of torsion, the lateral displacement of each point should also be measured. Lastly, there appears to be a significant amount of coupling with the landing skids in the model. Interference with a mode of the skids could change the torsional mode shape.

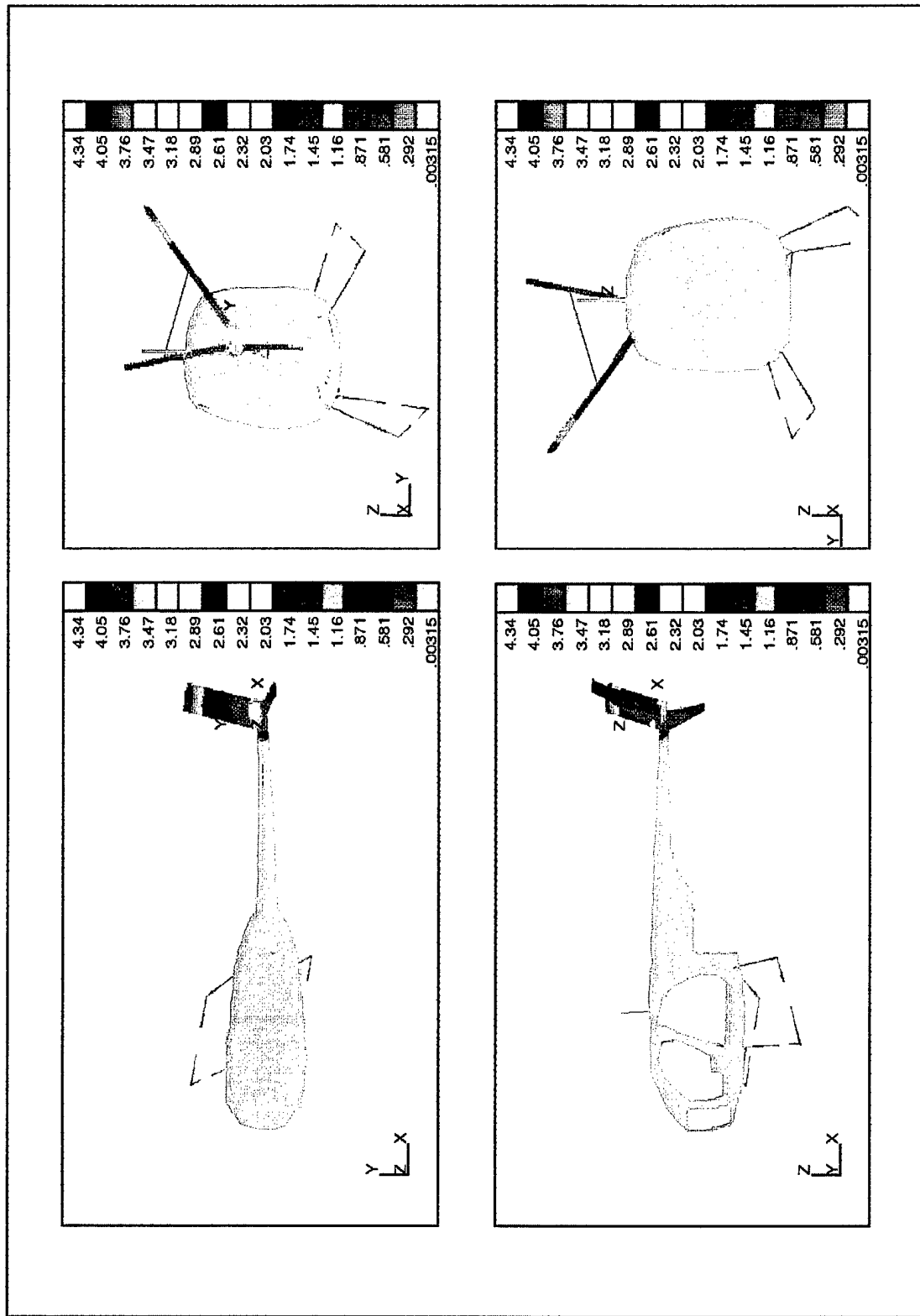


Figure 6.7. First Torsional Mode Shape at 15.40 Hz.

VII. CONCLUSIONS AND RECOMMENDATIONS

A. CONCLUDING REMARKS

The development of a finite element model is essential in the study of vibration response of complex structures such as modern military helicopters. Reduction of the vibration levels of helicopters is of significant concern as aircraft become more complex and vibration sensitive high-tech avionics become more critical to completion of the aircraft's primary mission.

The relative simplicity of the OH-6A airframe coupled with well documented response characteristics make this an ideal aircraft to study. A full-scale vibration test of the helicopter at NPS established the natural frequencies and mode shapes between 0 and 45 Hz. This thesis continues with that research and develops a FEM which is closely correlated to the experimental data. The increased understanding of OH-6A dynamic characteristics which this research creates further increases the capabilities of the school to conduct helicopter dynamics research. Furthermore, it enhances the prestige of NPS as a rotorcraft research facility.

Helicopters experience vibrations from a few primary sources. Vibrations transmitted through the main and tail rotors are the largest source. They occur primarily at 1P and NP frequencies. Higher frequency vibrations are a concern as well. They are associated with internal machinery such as engines and transmission components.

Additionally, random aerodynamic excitations from wind and rotor wash impingement on the fuselage can also have an effect.

When developing a FEM, it is necessary to realize that a finite element model is not an exact representation of the actual structure. There are errors associated with the discretization and interpolation of the structure. This error can be minimized by including a large number of very small elements in the FEM. The errors for the higher frequency modes will always be greater than the lower modes due to their complex mode shapes. It is, therefore, the goal of the engineer to develop a model which is accurate below a certain frequency level of interest.

A typical FEM consists of both a stiffness model and a mass model. The development of both of these components for this project was complicated by the lack of accurate structural design data for the helicopter. The structural components were created using external measurements of the test platform at NPS. The nose and empennage section were created using this method. The remainder of the aircraft is based on a FEM of a similar aircraft which was provided by McDonnell Douglas. The mass model was created using a point mass with rotational components placed near the C.G. of the empennage. The mass components were calculated using a design sensitivity approach.

Model frequencies correlated very closely to the test frequencies, especially in the lower frequency modes. The mode shapes did not correlate as well. Mode shapes were compared using the modal assurance criterion. Prior to performing the MAC, analytical mode shapes were reduced to the same size as the test modes using the NASTRAN built-

in static reduction method. The drastic reduction in the number of DOF introduced a great deal of error in the resulting test analysis model. It was more pronounced in the lateral modes than in the vertical. The torsional mode shape was the least correlated of them all. However, the general shape of all modes was similar by visual inspection. This leads to the conclusion that greater detail in the experimental mode shapes may give better correlation results.

B. RECOMMENDATIONS FOR FURTHER STUDY

The finite element model created for this project correlates well with the experimental data. It is a useful tool for further research in helicopter dynamics. It can be used to provide a basic knowledge of the process required to develop complex finite element models. There are, however, still some improvements which can be made which will increase its accuracy.

1. Improvements in the Experimental Data

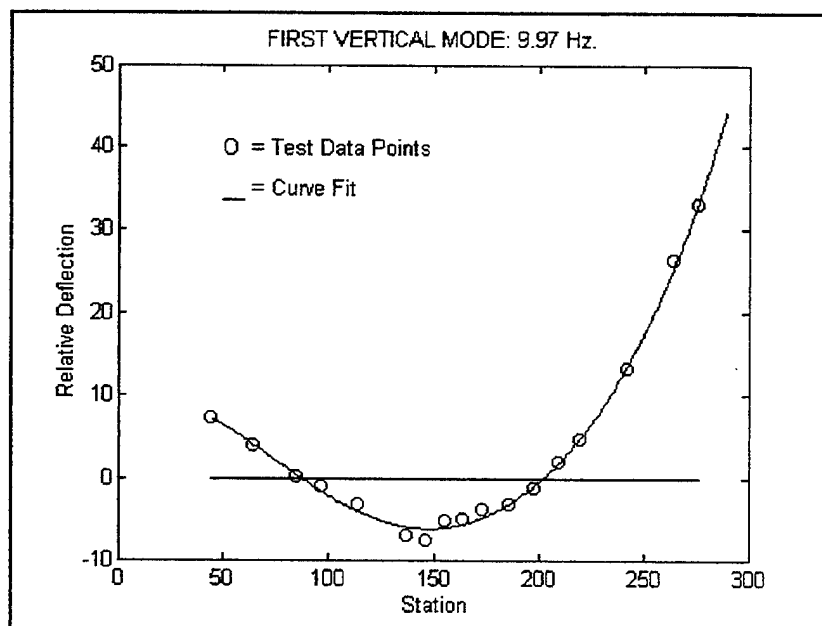
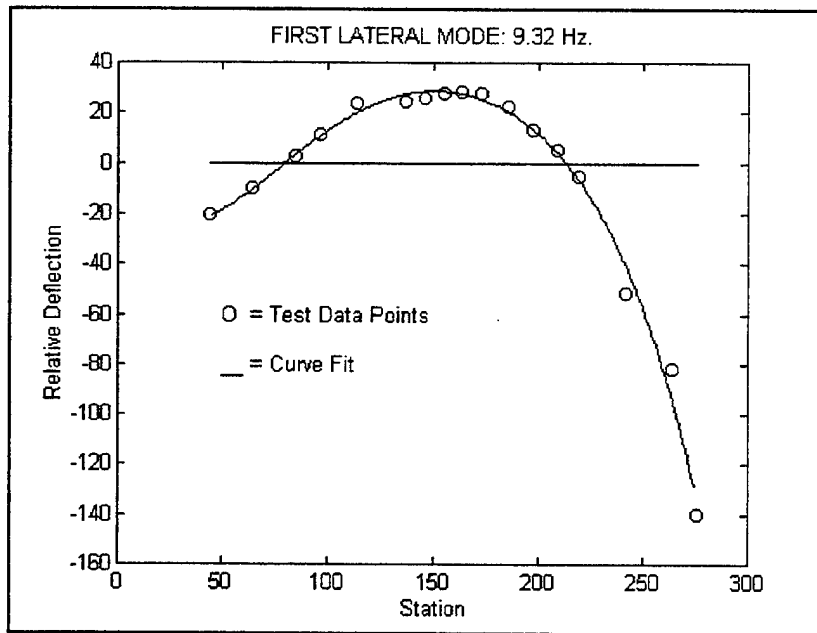
Experimental mode shapes were developed using between 17 and 19 data points. The analytical model contains 4398 DOF. The static reduction creates some rather large errors when reducing by such a significant amount. Taking measurements at additional data points would give more reliable experimental mode shapes. Additionally, torsional data was determined using only vertical displacement. Putting additional accelerometers on the tail to obtain lateral-vertical coupling by simultaneously measuring vertical-lateral movement would greatly enhance the accuracy of the test.

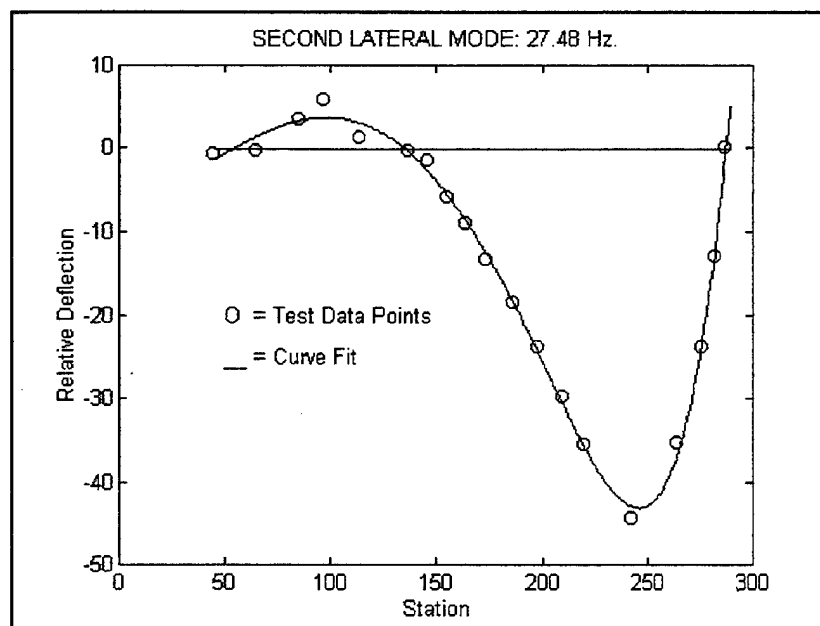
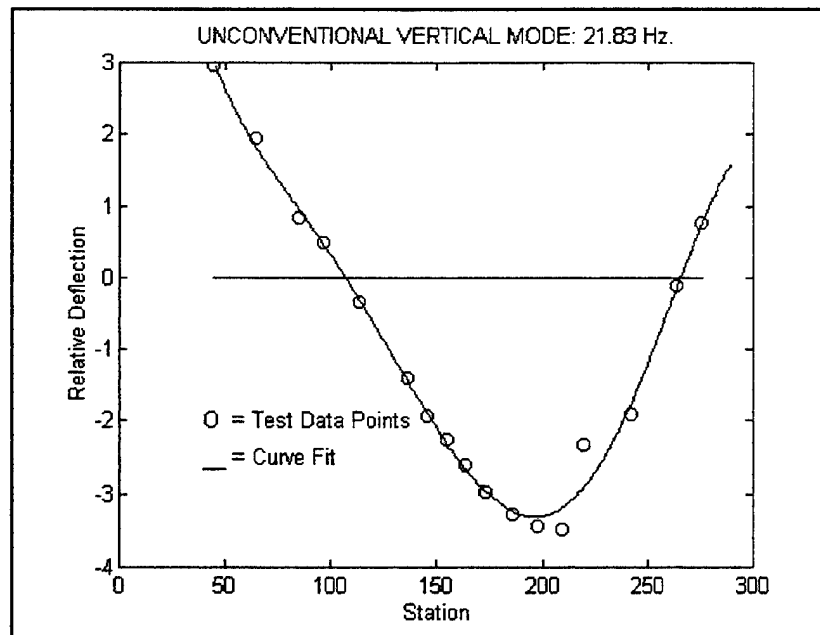
2. Improvements in the FEM

One area of potential error which was not addressed in this thesis is the landing skids. Landing skids on helicopters with more than two blades have pre-loaded springs and oleo dampers in order to eliminate ground resonance. The skids appear to play a significant role in the vibration response of several modes in this model. It is possible that the skids in the FEM do not accurately represent the OH-6A skids. It may be useful to model the skids with more accuracy. This could reduce the error in both the torsional mode and the second lateral mode.

There is also some discrepancy in the mass and C.G. of the model. This could have contributed to the errors in some of the mode shapes. Without accurate weight data it is an extremely difficult task to track down the discrepancies between the test platform and the model. If more accurate weight data is required, a sensitivity analysis could be performed on the entire airframe using the built-in capabilities of NASTRAN.

APPENDIX A. EXPERIMENTAL MODE SHAPE PLOTS





APPENDIX B. MODE SHAPE EXTRACTION PROGRAM

```
% shapes.m reads the mode shapes from an op4 file for computation in MATLAB.  
% Written by Lt. Mike Pampalone, Naval Postgraduate School
```

```
clear
```

```
% Get filename and open file  
filename=input('Enter the name of the NASTRAN op4 file>> ','s');  
[fid,message]=fopen(filename,'rt');  
if message~=""  
    disp(' Problem opening file. Check path/directory.')  
else  
    disp(' File opened successfully. Reading Data...')
```

```
% See end of file for closing "end" statement  
exit=1;  
cnt_lines=0;  
n=1;  
last_line=0;
```

```
% Two while loops. This allows program to break from the inner loop while  
% continuing to loop through lines of the op2 file. The file breaks from  
% the outer loop when end of file is detected.
```

```
while exit
```

```
    while 1  
        next_line=fgetl(fid);  
        cnt_lines=cnt_lines+1;
```

```
% Look for end of file  
    if ~isstr(next_line)  
        exit=0;  
        break  
    end
```

```
% Read first line of file  
    if(cnt_lines==1)
```

```

        modes=eval(['[',next_line(1:8),']']);
        DOF=eval(['[',next_line(9:16),']']);
        mode=0;
        break
    end

% Find the new mode number. The previous mode shape is evaluated to determine
% if the correct number of lines have been read. If not, it is padded
% with zeros. Next, the new mode shape is evaluated to determine if there are
% leading zeros. If so, it is padded. The index and mode number are then
% reset.
    if(eval(['[',next_line(1:8),']'])==(mode+1));
        if(last_line~=n-1)
            mode_shape(n:last_line,mode)=zeros(1:last_line+1-n,1);
        end
        mode=mode+1;
        n=1;
        first_line=eval(['[',next_line(9:16),']']);
        if(first_line~=1)
            mode_shape(1:3*first_line-3,mode)=zeros(1:3*first_line-3,1);
            n=3*first_line-2;
        end
        last_line=eval(['[',next_line(17:24),']']);
        break
    end

% If none of the above conditions are met, the line is written to the
% mode shape matrix in a column. Each column represents a different
% mode.
    mode_shape(n,mode)=eval(['[',next_line(1:21),']']);
    mode_shape(n+1,mode)=eval(['[',next_line(22:42),']']);
    mode_shape(n+2,mode)=eval(['[',next_line(43:63),']']);
    n=n+3;

end
end
fclose(fid);
disp('End of file detected. File closed.')

end

```

APPENDIX C. REDUCED MODE SHAPE DATA

% Reduced Analytical First Vertical Mode Shape

Vert1=[0.3803;0.2230;0.0673;-0.0201;-0.1525;-0.3473;-0.2892;-0.2985;...
-0.2973;-0.2959;-0.2881;-0.2548;-0.1520;-0.0374;0.3518;0.9097;1.2407];

% Reduced Analytical Second Vertical Mode Shape

Vert2=[-0.1014;-0.0453;0.0043;0.0349;0.0855;0.1326;0.1751;0.1972;...
0.2173;0.2370;0.2611;0.2774;0.2727;0.2592;0.1840;0.0483;-0.0335];

% Reduced Analytical Aft Vertical Mode Shape

VertA=[-0.0570;-0.0647;-0.0822;-0.0912;-0.1063;-0.1344;-0.1381;-0.1471;...
-0.1552;-0.1632;-0.1726;-0.1764;-0.1653;-0.1491;-0.0848;0.0169;0.0742];

% Reduced Analytical First Lateral Mode Shape

Lat1=[0.1795;0.1030;0.0252;-0.0183;-0.0828;-0.1454;-0.1320;-0.1426;...
-0.1513;-0.1528;-0.1454;-0.1298;-0.0979;-0.0615;0.0490;0.2003;0.2778];

% Reduced Analytical Second Lateral Mode Shape

Lat2=[0.0876;0.0333;-0.0453;-0.0804;-0.1275;-0.0657;0.2325;0.2717;0.3088;...
0.3376;0.3688;0.3822;0.3800;0.3616;0.2540;0.0550;-0.0336];

Reduced Analytical First Torsional Mode Shape (Vertical Deflection Only)

Tor1=[0.0902;0.0787;0.0689;0.0626;0.0498;0.0936;0.2806;0.6220];

% Experimental First Vertical Mode Shape

EVert1=[7.2153;3.8583;.232e-3;-1.0109;-3.3242;-7.0845;...
-7.6948;-5.1967;-5.0398;-3.874;-3.3242;-1.2556;1.82016;...
4.69972;13.2098;26.2452;32.9155];

% Experimental Second Vertical Mode Shape

EVert2=[2.9556;1.9342;.832;.490;-3.347;-1.4015;-1.9482;-2.268;-2.6158; ...
-2.9733;-3.2916;-3.455;-3.4877;-2.3296;-1.9118;-.110;.769];

% Experimental First Lateral Mode Shape

ELat1=[-20.839;-9.8965;2.0534;11.1376;23.564;24.2915;25.7875;27.7057;...
28.4033;27.6185;22.117;12.69;5.1226;-5.58;-51.8801;-82.343;-140.19];

% Experimental Second Lateral Mode Shape

ELat2=[-.616;-.343;3.42016;5.8998;1.28174;-.217;-1.4801;-5.891;-9.0354;...
-13.411;-18.55;-23.913;-29.82;-35.586;-44.425;-35.444;-23.956];

% Experimental First Torsional Mode Shape (Vertical Deflection only)

% Horizontal Stab

% 13.079;-33.243;-91.553;-168.94;-235.75;

% Stations along horizontal stab

% 7.25 22.75 38 50.75 65.75

% Vertical Stabs

% 103.379;80.544;60.2861;37.886;12.0763;-24.937;-75.204;-151.72];

% Stations along vertical stab

% -28.5 -20.5 -12.5 -4.5 7.5 20.5 33.5 51.5

% Data points truncated and ordered to match analytical set

ETor=[-151.7200;-75.2040;12.0763;37.886;103.3790;13.0790;-91.5530;-235.7500];

phi_exp=[ELat1,EVert1,EVert2,ELat2];

phi_anal=[Lat1,Vert1,Vert2,Lat2];

MAC1 =

0.7038	0.9476	0.0529	0.0164
0.6227	0.9209	0.0100	0.0000
0.5533	0.2067	0.9026	0.7022
0.0003	0.1106	0.5029	0.5440

phi_tor_exp=ETor;

phi_tor_anal=Tor1;

MAC2 =

0.6331

APPENDIX D. MAC CALCULATION PROGRAM

```
% fmac.m
% This function calculates the MAC matrix for a matrix onto itself
% [mac(a,a)] use mac = fmac(a)
% or between two matrices.
% [mac(a,b)] use mac = fmac(a,b)
% Written by Professor Josh Gordis, Naval Postgraduate School

function [mac]=fmac(a,b);
asize=size(a);
nacols=asize(1,2);
if nargin == 1;
    b = a;
    nbcols = nacols;
else
    bsize=size(b);
    nbcols=bsize(1,2);
end;
for i=1 : nacols;
    for j= 1 : nbcols;
        top = ( a(:,i)' * b(:,j) )^2;
        bottom = ( a(:,i)' * a(:,i) ) * ( b(:,j)' * b(:,j) );
        mac(i,j) = top / bottom;
    end
end
```


APPENDIX E. NASTRAN FORMATTED EMPENNAGE DATA

\$ OH-6A NASTRAN FEM modified empennage data. This was modified by Lt. Michael
\$ Pampalone, USN, Naval Postgraduate School, 12 August 1996.

\$

\$

\$***** MODIFIED TAIL *****

\$

\$ BEGIN VERTICAL STABILIZER

\$

\$.....1.....2.....3.....4.....5.....6.....7.....8.....9.....10

CORD2R 301 273.90 0.0 54.358 273.90 0.0 55.0+CD301

+CD301 274.5 0.0 54.358

\$

\$ VERTICAL STABILIZER - TOP

GRID	31018	301	0.	0.	3.383
GRID	31020	301	2.127	1.	3.280
GRID	31022	301	2.127	-1.	3.280
GRID	31024	301	6.55	1.	3.067
GRID	31025	301	6.55	0.	3.067
GRID	31026	301	6.55	-1.	3.067
GRID	31028	301	14.98	0.	2.66
GRID	31030	301	1.47	0.	6.32
GRID	31032	301	3.60	1.	6.21
GRID	31034	301	3.60	-1.	6.21
GRID	31036	301	7.756	1.	6.01
GRID	31038	301	7.756	-1.	6.01
GRID	31040	301	15.99	0.	5.615
GRID	31042	301	15.64	0.	31.54
GRID	31044	301	16.38	1.	31.51
GRID	31046	301	16.38	-1.	31.51
GRID	31048	301	18.17	1.	31.42
GRID	31050	301	18.17	-1.	31.42
GRID	31052	301	24.66	0.	31.11
GRID	31054	301	22.75	0.	48.47
GRID	31056	301	24.89	1.	48.37
GRID	31058	301	24.89	-1.	48.37
GRID	31060	301	25.12	1.	48.35
GRID	31062	301	25.12	-1.	48.35
GRID	31064	301	30.46	0.	48.10

\$

\$ VERTICAL STABILIZER - BOTTOM

GRID	31066	301	0.	0.	-3.383
GRID	31068	301	2.13	1.	-3.339
GRID	31070	301	2.13	-1.	-3.339
GRID	31072	301	6.55	1.	-3.247
GRID	31073	301	6.55	0.	-3.247
GRID	31074	301	6.55	-1.	-3.247
GRID	31076	301	12.0	0.	-3.134
GRID	31078	301	12.21	0.	-26.76
GRID	31080	301	13.36	1.	-26.72
GRID	31082	301	13.36	-1.	-26.72
GRID	31084	301	15.12	1.	-26.70
GRID	31086	301	15.12	-1.	-26.70
GRID	31088	301	17.68	0.	-26.65

\$

\$ FWD SPAR - VERT. STAB.

CROD	10403	11030	31056	31044		
CROD	10404	11036	31044	31032		
CROD	10405	11042	31032	31020		
CROD	10406	11030	31058	31046		
CROD	10407	11036	31046	31034		
CROD	10408	11042	31034	31022		
CROD	10409	11030	31068	31080		
CROD	10410	11030	31070	31082		
CSHEAR	40483	14040	31056	31058	31046	31044
CSHEAR	40484	14048	31044	31046	31034	31032
CSHEAR	40485	14055	31032	31034	31022	31020
CSHEAR	40486	14040	31068	31070	31082	31080

\$

\$ AFT SPAR - VERT. STAB.

CROD	10411	11030	31060	31048		
CROD	10412	11044	31048	31036		
CROD	10413	11057	31036	31024		
CROD	10414	11030	31062	31050		
CROD	10415	11044	31050	31038		
CROD	10416	11057	31038	31026		
CROD	10417	11030	31072	31084		
CROD	10418	11030	31074	31086		
CSHEAR	40487	14040	31060	31062	31050	31048
CSHEAR	40488	14058	31048	31050	31038	31036
CTRIA3	30124	13071	31036	31038	31025	

CTRIA3 30125 13071 31024 31025 31036
 CTRIA3 30126 13071 31026 31025 31038
 CTRIA3 30127 13071 31084 31086 31073
 CTRIA3 30128 13071 31072 31073 31084
 CTRIA3 30129 13071 31074 31073 31086

\$

\$ TOP VERT. STAB. LOWER END CAP

CBAR 20403 12014 31018 31020 31028
 CBAR 20404 12014 31018 31022 31028
 CROD 10419 11298 31020 31022
 CBAR 20405 12298 31020 31024 31028
 CBAR 20406 12298 31022 31026 31028
 CBAR 20407 12298 31024 31025 31036
 CBAR 20408 12298 31026 31025 31038
 CBAR 20409 12014 31024 31028 31018
 CBAR 20410 12014 31026 31028 31018
 CTRIA3 30130 13025 31018 31020 31022
 CSHEAR 40489 14250 31020 31022 31026 31024
 CTRIA3 30131 13025 31024 31026 31028

\$

\$ TOP VERT. STAB. LOWER RIB

CBAR 20411 12014 31030 31032 31040
 CBAR 20412 12014 31030 31034 31040
 CROD 10420 11298 31032 31034
 CBAR 20413 12014 31032 31036 31040
 CBAR 20414 12014 31034 31038 31040
 CROD 10421 11298 31036 31038
 CBAR 20415 12014 31036 31040 31030
 CBAR 20416 12014 31036 31040 31030

\$

\$ TOP VERT. STAB. INTERMEDIATE RIB

CBAR 20417 12014 31042 31044 31052
 CBAR 20418 12014 31042 31046 31052
 CROD 10422 11298 31044 31046
 CBAR 20419 12014 31044 31048 31052
 CBAR 20420 12014 31046 31050 31052
 CROD 10423 11298 31048 31050
 CBAR 20421 12014 31048 31052 31042
 CBAR 20422 12014 31050 31052 31042

\$

\$ TOP VERT. STAB. UPPER END CAP

CBAR	20423	12014	31054	31056	31064	
CBAR	20424	12014	31054	31058	31064	
CROD	10424	11298	31056	31058		
CBAR	20425	12298	31056	31060	31064	
CBAR	20426	12298	31058	31062	31064	
CROD	10425	11298	31060	31062		
CBAR	20427	12014	31060	31064	31054	
CBAR	20428	12014	31062	31064	31054	
CTRIA3	30132	13025	31054	31056	31058	
CSHEAR	40490	14250	31056	31058	31062	31060
CTRIA3	30133	13025	31060	31062	31064	

\$

\$ BOTTOM VERT. STAB. LOWER END CAP

CBAR	20429	12017	31078	31080	31088	
CBAR	20430	12017	31078	31082	31088	
CROD	10426	11120	31080	31082		
CBAR	20431	12120	31080	31084	31088	
CBAR	20432	12120	31082	31086	31088	
CROD	10427	11120	31084	31086		
CBAR	20433	12017	31084	31088	31078	
CBAR	20434	12017	31086	31088	31078	
CTRIA3	30134	13025	31078	31080	31082	
CSHEAR	40491	14250	31080	31082	31086	31084
CTRIA3	30135	13025	31084	31086	31088	

\$

\$ BOTTOM VERT. STAB. UPPER END CAP

CBAR	20435	12017	31066	31068	31076	
CBAR	20436	12017	31066	31070	31076	
CROD	10428	11120	31068	31070		
CBAR	20437	12298	31068	31072	31076	
CBAR	20438	12298	31070	31074	31076	
CBAR	20439	12298	31072	31073	31084	
CBAR	20440	12298	31074	31073	31086	
CBAR	20441	12017	31072	31076	31066	
CBAR	20442	12017	31074	31076	31066	
CTRIA3	30136	13025	31066	31068	31070	
CSHEAR	40492	14250	31068	31070	31074	31072
CTRIA3	30137	13025	31072	31074	31076	

\$

\$ SKIN

CSHEAR	40493	14032	31056	31044	31048	31060
--------	-------	-------	-------	-------	-------	-------

CSHEAR	40494	14032	31058	31046	31050	31062
CSHEAR	40495	14032	31044	31032	31036	31048
CSHEAR	40496	14032	31046	31034	31038	31050
CSHEAR	40497	14032	31032	31020	31024	31036
CSHEAR	40498	14032	31034	31022	31026	31038

\$

CSHEAR	40499	14032	31068	31080	31084	31072
CSHEAR	40500	14032	31070	31082	31086	31074

\$

CSHEAR	40501	14020	31066	31068	31080	31078
CSHEAR	40502	14020	31066	31070	31082	31078

\$

CSHEAR	40503	14020	31076	31072	31084	31088
CSHEAR	40504	14020	31076	31074	31086	31088

\$

CSHEAR	40505	14020	31054	31042	31044	31056
CSHEAR	40506	14020	31054	31042	31046	31058
CSHEAR	40507	14020	31042	31030	31032	31044
CSHEAR	40508	14020	31042	31030	31034	31046
CSHEAR	40509	14020	31030	31018	31020	31032
CSHEAR	40510	14020	31030	31018	31022	31034

\$

CSHEAR	40511	14020	31064	31060	31048	31052
CSHEAR	40512	14020	31064	31062	31050	31052
CSHEAR	40513	14020	31052	31048	31036	31040
CSHEAR	40514	14020	31052	31050	31038	31040
CSHEAR	40515	14020	31040	31036	31024	31028
CSHEAR	40516	14020	31040	31038	31020	31028

\$

\$ HORIZONTAL STABILIZER

\$

GRID	32002	301	0.0	3.383	0.0
GRID	32004	301	6.55	2.60	0.74
GRID	32005	301	6.55	3.157	-0.09
GRID	32006	301	6.56	3.72	-0.92
GRID	32008	301	11.16	2.44	0.68
GRID	32010	301	11.19	3.56	-0.98
GRID	32012	301	17.74	2.77	-0.24
GRID	32014	301	0.13	6.28	1.95
GRID	32016	301	6.67	5.49	2.69
GRID	32018	301	6.69	6.61	1.03

GRID	32020	301	11.30	5.33	2.63
GRID	32022	301	11.32	6.45	0.97
GRID	32024	301	17.86	5.67	1.71
GRID	32026	301	1.23	31.60	18.91
GRID	32028	301	7.78	30.82	19.65
GRID	32030	301	7.79	31.94	17.99
GRID	32032	301	12.41	30.65	19.58
GRID	32034	301	12.42	31.78	17.92
GRID	32036	301	18.97	30.99	18.66
GRID	32038	301	2.29	55.89	35.19
GRID	32040	301	8.84	55.11	35.93
GRID	32042	301	8.86	56.23	34.27
GRID	32044	301	13.47	54.95	35.86
GRID	32046	301	13.49	56.07	34.20
GRID	32048	301	20.03	55.28	34.94

\$

\$ FWD SPAR

CROD	10430	11030	32004	32016
CROD	10431	11030	32016	32028
CROD	10432	11030	32028	32040

\$

CROD	10433	11030	32006	32018
CROD	10434	11030	32018	32030
CROD	10435	11030	32030	32042

\$

CSHEAR	40520	14040	32004	32006	32018	32016
CSHEAR	40521	14040	32016	32018	32030	32028
CSHEAR	40522	14040	32028	32030	32042	32040

\$

\$ AFT SPAR

CROD	10436	11030	32008	32020
CROD	10437	11030	32020	32032
CROD	10438	11030	32032	32044

\$

CROD	10439	11030	32010	32022
CROD	10440	11030	32022	32034
CROD	10441	11030	32034	32046

\$

CSHEAR	40523	14040	32008	32010	32022	32020
CSHEAR	40524	14040	32020	32022	32034	32032
CSHEAR	40525	14040	32032	32034	32046	32044

\$

\$ INBOARD END CAP

CBAR	20445	12067	32002	32004	32006
CBAR	20446	12177	32004	32008	32006
CBAR	20447	12067	32008	32012	32006
CBAR	20448	12067	32012	32010	32004
CBAR	20449	12177	32010	32006	32004
CBAR	20450	12067	32006	32002	32004
CROD	10442	11020	32004	32005	
CROD	10443	11020	32005	32006	
CROD	10444	11020	32008	32010	
CTRIA3	30140	15032	32004	32005	32002
CTRIA3	30142	15032	32005	32006	32002
CTRIA3	30143	15032	32004	32005	32008
CTRIA3	30144	15032	32005	32006	32010
CTRIA3	30145	15032	32008	32010	32006
CTRIA3	30146	15032	32008	32010	32012

\$

\$ INBOARD RIB

CBAR	20451	12014	32014	32016	32024
CBAR	20452	12014	32016	32020	32024
CBAR	20453	12014	32020	32024	32014
CBAR	20454	12014	32024	32022	32014
CBAR	20455	12014	32022	32018	32024
CBAR	20456	12014	32018	32014	32024
CROD	10445	11018	32016	32018	
CSHEAR	40526	14025	32016	32020	32022 32018
CTRIA3	30147	13025	32014	32016	32018
CTRIA3	30148	13025	32020	32022	32024

\$

\$ INTERMEDIATE RIB

CBAR	20457	12014	32026	32028	32036
CBAR	20458	12014	32028	32032	32036
CBAR	20459	12014	32032	32036	32026
CBAR	20460	12014	32036	32034	32026
CBAR	20461	12014	32034	32030	32036
CBAR	20462	12014	32030	32026	32036
CROD	10446	11018	32028	32030	
CSHEAR	40527	14025	32028	32032	32034 32030
CTRIA3	30149	13025	32026	32028	32030
CTRIA3	30150	13025	32032	32034	32036

\$

\$ OUTBOARD END CAP

CBAR	20463	12022	32038	32040	32048	
CBAR	20464	12022	32040	32044	32048	
CBAR	20465	12022	32044	32048	32042	
CBAR	20466	12022	32048	32046	32038	
CBAR	20467	12022	32046	32042	32048	
CBAR	20468	12022	32042	32038	32048	
CROD	10447	11018	32040	32042		
CSHEAR	40528	14040	32040	32044	32046	32042
CTRIA3	30151	15040	32040	32042	32038	
CTRIA3	30152	15040	32044	32046	32048	

\$

\$ SKIN

CROD	10448	11016	32012	32024		
CROD	10449	11016	32024	32036		
CROD	10450	11016	32036	32048		
CSHEAR	40529	14020	32002	32004	32016	32014
CSHEAR	40530	14020	32004	32008	32020	32016
CSHEAR	40531	14020	32008	32012	32024	32020
CSHEAR	40532	14020	32002	32006	32018	32014
CSHEAR	40533	14020	32006	32010	32022	32018
CSHEAR	40534	14020	32010	32012	32024	32022

\$

CSHEAR	40535	14020	32014	32016	32028	32026
CSHEAR	40536	14020	32016	32020	32032	32028
CSHEAR	40537	14020	32020	32024	32036	32032
CSHEAR	40538	14020	32014	32018	32030	32026
CSHEAR	40539	14020	32018	32022	32034	32030
CSHEAR	40540	14020	32022	32024	32036	32034

\$

CSHEAR	40541	14020	32026	32028	32040	32038
CSHEAR	40542	14020	32028	32032	32044	32040
CSHEAR	40543	14020	32032	32036	32048	32044
CSHEAR	40544	14020	32026	32030	32042	32038
CSHEAR	40545	14020	32030	32034	32046	32042
CSHEAR	40546	14020	32034	32036	32048	32046

\$

\$ CONNECTION BETWEEN VERTICAL STAB. AND TAILBOOM

\$

RBAR	50003	27302	31018	123456	123456
------	-------	-------	-------	--------	--------

RBAR	50004	28002	31025	123456	123456
RBAR	50005	28010	31073	123456	123456
RBAR	50006	27310	31066	123456	123456

\$

\$ CONNECTION BETWEEN HORIZONTAL STAB. AND TAILBOOM

\$

RBAR	50007	27306	32002	123456	123456
RBAR	50008	28006	32005	123456	123456

\$

\$ CONNECTING STRUT BETWEEN VERTICAL AND HORIZONTAL STABS.

CBAR	20469	12022	32028	31048	31050
------	-------	-------	-------	-------	-------

\$

\$ ***** MODIFIED TAIL SECTION MASS *****

CMASS1	6320221	6320221	32022	1
CMASS1	6320222	6320221	32022	2
CMASS1	6320223	6320221	32022	3
CMASS1	6320224	6320224	32022	4
CMASS1	6320225	6320225	32022	5
CMASS1	6320226	6320226	32022	6
PMASS	6320221	38.0		
PMASS	6320224	100.0		
PMASS	6320225	524.0		
PMASS	6320226	600.0		

LIST OF REFERENCES

1. *Aviation Unit and Intermediate Maintenance Manual: Helicopter, Observation OH-6A*. Headquarters, Department of the Army, Washington, DC. 1981.
2. Ferg, D. and Toossi, M. *NASA Contractor Report 187449: Finite Element Modeling of the Higher Harmonic Control OH-6A Helicopter Airframe*. National Aeronautics and Space Administration, Hampton, VA. October 1990.
3. Harris, J. H. *Preliminary Vibration Survey of a Suspended Full-Scale OH-6A Helicopter from 0 to 45 Hz*. Master's Degree Thesis. Naval Postgraduate School, Monterey, CA. March 1996.
4. Wood, E. R. "An Introduction to Helicopter Dynamics." *An Introduction to Helicopter Engineering*. Hughes Helicopters, Inc. and Graduate Aeronautical Laboratories, California Institute of Technology. 1984.
5. Inman, D. J. *Engineering Vibration*. Prentice-Hall Inc. Englewood Cliffs, NJ. 1994.
6. Craig, R. R. Jr. *Structural Dynamics, An Introduction to Computer Methods*. John Wiley and Sons. New York, NY. 1981.
7. Gordis, J. H. Class Notes: ME4522, Shipboard Vibration and Noise. Naval Postgraduate School, Monterey, CA. October, 12 1996.
8. Ugural, A. C. and Fenster, S. K. *Advanced Strength and Applied Elasticity, Third Edition*. Prentice-Hall Ins. Englewood Cliffs, NJ. 1995.
9. Gordis, J. H. Class Notes: ME4522, Shipboard Vibration and Noise. Naval Postgraduate School, Monterey, CA. October 15, 1996.
10. *MSC/NASTRAN Quick Reference Guide, Version 68*. Reymond, M. and Miller, M., Ed. MacNeal Schwendler Corporation. Los Angeles, CA. 1994.
11. Ewins, D. J. *Modal Testing: Theory and Practice*. Research Studies Press, Ltd. Taunton, Somerset England. 1984.
12. Gordis, J. H. "An Analysis of the Improved Reduced System (IRS) Model Reduction Procedure," *Modal Analysis: The International Journal of Analytical and Experimental Modal Analysis*. Vol. 9, No. 4. October 1994. Pp. 269-285.

INITIAL DISTRIBUTION LIST

	No. Copies
1. Defense Technical Information Center 8725 John J. Kingman Rd., STE 0944 Ft. Belvoir, VA 22060-6218	2
2. Dudley Knox Library Naval Postgraduate School Monterey, CA 93943-5101	2
3. Department of Mechanical Engineering, Code ME Naval Postgraduate School Monterey, CA 93943-5000	2
4. Professor Joshua H. Gordis, Code ME/Go Department of Mechanical Engineering Naval Postgraduate School Monterey, CA 93943-5000	2
5. Professor E. Roberts Wood, Code AA/Wd Department of Aeronautics and Astronautics Naval Postgraduate School Monterey, CA 93943-5000	3
6. Professor Donald A. Danielson, Code MA/Dd Department of Mathematics Naval Postgraduate School Monterey, CA 93943-5000	1
7. LT Michael Pampalone 131 Leidig Cir. Monterey, CA 93940	2
8. Dr. Mustafa Toossi Manager, Airframe Dynamics McDonnell Douglas Helicopter Company 500 East McDowell Road Mesa, AZ 85215	1

9. Dr. Dana Taylor 1
Commander
U. S. Army ATCOM
ATTN: AMSAT-R-EAD
4300 Goodfellow Blvd.
St. Louis, MO 63120
10. Dr. Friedrich Straub 1
Research and Engineering Specialist
McDonnell Douglas Helicopter Company
500 East McDowell Road
Mesa, AZ 85215
11. Mr. Louis J. Silverthorn 1
Sr. Leader Rotor Dynamics
McDonnell Douglas Helicopter Company
500 East McDowell Road
Mesa, AZ 85215
10. Mr. Robert L. Tomaine 1
U. S. Army ATCOM
4300 Goodfellow Blvd.
St. Louis, MO 63120
11. Dr. Sam T. Crews 1
U. S. Army ATCOM
4300 Goodfellow Blvd.
St. Louis, MO 63120
12. Dr. Dev Banerjee 1
McDonnell Douglas Helicopter Company
500 East McDowell Road
Mesa, AZ 85215
13. Mr. Kenneth B. Amer 1
8025 Alverstone Avenue
Los Angeles, CA 90045